Spiral Antenna Design with MATLAB

Marcos Fioravante Buccella Espinoza

Master's Degree in Telecommunication Engineering
Antenna Technologies

FW Tutor Name
Dr. Jaume Anguera Pros
Dr. Aurora Andújar Linares
Teacher responsible for the course
Dr. Germán Cobo Rodríguez

01/2023

Universitat Oberta
de Catalunya

FINAL WORK SHEET

Title of the work:	*Spiral Antenna Design with MATLAB*
Author's name:	*Marcos F. Buccella Espinoza*
Consultant's name:	*Dr. Jaume Anguera Pros* *Dr. Aurora Andújar Linares*
TRC name:	*Dr. Germán Cobo Rodríguez*
Date of delivery (mm/yyyy):	*01/2023*
Degree or program:	*Master's Degree in Telecommunication Engineering*
Final Work Area:	*Antenna technologies*
Language of the work:	*English*
Keywords:	*Spiral, frequency-independent, simulation*

Abstract

This paper presents a quantitative analysis of spiral antennas based on designs and simulations performed in the MATLAB software suite. First, a thorough review of previous scientific literature used as a conceptual basis for the realization of this work is presented. Based on this review, the parameters of interest to be analyzed with this type of antennas are discussed and visualized in other types of spiral antennas to justify the choice of this type of spiral. Subsequently, the simulation process used to analyze various equiangular spiral antennas in MATLAB is described in detail. The first simulation is performed by adjusting the antenna dimensions based on a previously fixed operating frequency range and keeping the rest of the characteristics at their default value, from which several plots of relevant parameters are obtained, to be then analyzed. Subsequently, the effect of varying the number of turns of the equiangular spiral on the performance of the antenna in its operating frequency band is analyzed. Once the influence of this parameter has been verified, an optimization of the number of turns that maximizes the gain in the center of the operating frequency band is performed. Finally, the effects on the antenna radiation are evaluated by including an infinite reflector plane before it, generating an increase in the gain and a unidirectional radiation, but sacrificing stability in some of its parameters.

Resumen del Trabajo

Este documento presenta un análisis cuantitativo de las antenas de espiral a partir de diseños y simulaciones realizadas en la suite informática MATLAB. En primer lugar, se presenta una revisión profunda de bibliografía científica previa utilizada como base conceptual para la realización de este trabajo. En base a esta, se discuten los parámetros de interés que se desean analizar con

este tipo de antenas y se visualizan en otro tipo de antenas de espiral para justificar la elección de este tipo de espiral en particular. Posteriormente, se describe en detalle el proceso de simulación empleado para analizar diversas antenas de espiral equiangular en MATLAB. La primera simulación es realizada ajustando las dimensiones de la antena en base a un rango de frecuencias de operación previamente fijado y manteniendo el resto de las características en su valor por defecto, a partir de lo que se obtienen diversas gráficas de parámetros relevantes, para ser seguidamente analizados. Posteriormente, se analiza el efecto en el comportamiento de la antena en su banda frecuencial de operación al variar el número de vueltas que posee la espiral equiangular. Una vez comprobado la influencia de este parámetro, se realiza una optimización en el número de vueltas que maximiza la ganancia en el centro de la banda de frecuencias de operación. Finalmente, se evalúan los efectos en la radiación de la antena al incluir un plano reflector infinito anterior a esta, generando un incremento en la ganancia y una radiación unidireccional, pero sacrificando estabilidad en sus parámetros.

Index

List of figures

1. Introduction

1.1. Context and justification of the work

This project arises from the need to have a simulation system for spiral antennas that allows to obtain their parameters of interest in a simple way. Spiral antennas have numerous applications especially due to their frequency-independent behavior, so having a simulation software that allows easy modeling of them is necessary.

As the bandwidth in which these antennas operate is usually very high, the simulation process can be complex since the time and computational requirements are significantly increased based on the frequency range under study. Therefore, it is desired to test the usage of MATLAB to simulate this type of antennas, hoping to obtain graphical and data results that allows to analyze their performance in a relatively simple way.

1.2. Objectives of the work

The objectives of the work are as follows:

- To understand how spiral antennas work, with emphasis on the equiangular spiral type.
- To simulate different configurations of equiangular spiral antennas over a defined frequency range to determine the effect of the variation of their parameters on their radiation.
- To analyze the results obtained and determine if the chosen tool is suitable for this type of simulations.

1.3. Sustainability, social-ethical and diversity impact

The development of this work provides an insight into a type of antenna with a very high frequency range. This can provide a positive impact on sustainability, as its usage could incorporate several wireless communications applications within a single antenna, which could lead to a long-term reduction of waste and pollutants, as well as a better resource utilization.

1.4. Approach and method followed

The first part of the project was based on research into the operation and applications of this type of antenna in different scientific articles. Following this research, simulations have been carried out. To do this, codes available in the official MATLAB documentation are used, specifically in the documentation of its Antenna Toolbox. The parameters of these codes have been adjusted according to the need of the different simulations proposed in the development of the work. Once the code was generated, optimized, and debugged for the specific needs of this project, it was executed and tested for correct operation. Finally, the results have been compiled in this work.

1.5. Work Planning

The project has been divided into four main stages: a review of scientific bibliography and training, the analysis of spiral antennas, an analysis of the antenna with a resonant element and finally the documentation stage, as explained in the Gannt diagram from *Figure 1*. Throughout the project, routine meetings have been held with the tutor in charge of the work so that the project planning was fully followed.

Title	Start Time	End Time	Sep 15-20	11-17	18-24	25-01	Oct 02-08	09-15	16-22	23-29	30-05	Nov 06-12	13-19	20-26	27-03	Dec 04-10	11-17	18-24	25-31	01-07	08-14
Review Scientific Bibliography and Training	09/15/2022	11/01/2022																			
Scientific Bibliography review	09/15/2022	10/10/2022																			
MATLAB Antenna Toolbox training	10/10/2022	11/01/2022																			
Analysis of a spiral antenna	10/15/2022	11/15/2022																			
First simulations	10/15/2022	10/30/2022																			
Optimization and improvements	10/30/2022	11/15/2022																			
Analysis of a spiral antenna having a cavity underneath	11/15/2022	12/15/2022																			
Basic reflector antenna simulations	11/15/2022	11/30/2022																			
Integration with a equiangular spiral	11/30/2022	12/15/2022																			
Documentation	12/15/2022	01/15/2023																			

Figure 1: Gantt chart of the project

The first stage consisted of laying the theoretical foundations for the project. First, the basic operation of spiral antennas was analyzed. Subsequently, a review of scientific articles was carried out and a total of ten were selected. From these, a summary was made from which various applications and improvements provided by this type of antennas were extracted. This task was completed on October 10, 2022. Next, the operation of the MATLAB Antenna Toolbox was analyzed and a process of familiarization and learning of its operation was carried out. This stage was concluded on November 1, 2022.

The next stage began immediately upon completion of the first stage. It began with a basic simulation of an equiangular spiral antenna for a defined frequency range. Various parameters such as radiation patterns, input impedance, S_{11} parameter, among others, were obtained. A rectangular spiral antenna was also analyzed and compared with the equiangular antenna. This activity was completed on October 30, 2022. Then, an antenna optimization process was performed based on the analysis of the importance of the rate of increase in equiangular spiral antennas. This stage was completed on November 15, 2022.

The third stage consisted of analyzing the impact of adding a reflector plane under the antenna. First, a practical study of simulating reflector planes on arbitrary antennas and observing their performance was carried out. Once the use of this type of elements was understood, it was integrated with the optimized equiangular spiral antenna obtained in the second stage. This stage was completed on December 15, 2022.

Finally, the documentation stage of the work was carried out. In this stage, this thesis was written as a product of the compilation of the work done in the previous months. The procedures and results obtained were integrated in the format provided by the Universitat Oberta de Catalunya. At the same time, we worked on a presentation with slides where an explanation of the work carried out was made. Each of the stages of this project were integrated in a summarized but sufficiently detailed way for its presentation and final defense. This stage closes the project and was concluded on January 15, 2022.

1.6. Summary of products obtained

At the end of this project, it is expected to obtain:

- A literature review of the characteristics and applications of equiangular spiral antennas.
- The lines of code used to perform simulations with equiangular and rectangular spiral antennas.
- The results of the simulations presented graphically.

1.7. Brief description of the other chapters of the report

Chapter two is divided into a literature review and a simulation stage. The first part is divided into a review of the basic operation of equiangular spiral antennas and the summary of ten different scientific articles related to these antennas, detailing applications, improvements, and characteristics of this type of antennas. The next part of the chapter focused on the simulation of different spiral antennas. First, a simple equiangular spiral antenna was simulated and compared with a rectangular spiral antenna of similar characteristics to justify the choice of the former. Then, the influence of one of its parameters has been studied and an optimization process has been performed to this parameter. Finally, the effect of including a reflector plane in the antenna performance has been studied.

The same chapter details all the results obtained for each case. The findings are presented graphically and include a detailed analysis of the results obtained. Each result appears after the code to generate them. Chapter three contains the conclusions obtained from this work, answering the questions posed previously. The chapter four contains a list of acronyms used in the development of the work. The chapter five lists the bibliography consulted for the execution of this project. Finally, the sixth chapter includes a small manual on the use of the MATLAB antenna optimization tool and a code used in the second chapter that was too long to be included in the paper.

2. Materials, methods, and results

2.1. Frequency-independent antennas principles

Commonly, antenna parameters – like the radiation pattern, gain, and input impedance - are a function of their dimensions expressed in λ. In fact, if all the dimensions of a structure operating at a frequency f are scaled by a factor τ, the resulting antenna will have the same parameters at a frequency f/τ. This property (known as the similarity principle) can be rigorously demonstrated and is sometimes used to build and measure scale models. It was also demonstrated (Rumsey, 1957) to establish the principle on which frequency-independent antennas are based: if an antenna is self-scalable, that is, it becomes itself under any arbitrary scaling factor τ, its properties will be independent of frequency.

Self-scaling structures are defined only by angles (equiangular structures) and extend in principle from a null expansion point to infinity. The simplest example is the biconical antenna (a simple dipole with infinite conical arms), however, when this structure is truncated to a certain size, its properties vary with frequency. This happens because this antenna is not truncable (another requirement for frequency independence), since its traveling-wave current has a constant value which is independent of the distance to the excitation point. This can be verified by modelling this type of antenna as an infinite TEM line (Aznar, Roca, Casals, Robert, & Boris, 2002).

Truncable structures display a property in which the surface currents decay relatively fast with distance (relative to the excitation point), so that the infinite self-scalable structure can be trimmed by two spheres that adjust the theoretical infinite band of operation to a smaller one, bound by the frequencies f_{max} and f_{min}, related respectively to the radii of these spheres. The upper frequency f_{max} is limited by the physical size to be given to the excitation connection terminals around the expansion point. On the other hand, the lower f_{min} is conditioned by the outer radius of the truncation (physical size of the antenna) and corresponds to the one that makes the current reach an appreciable value in this outer zone.

Another concept that provides frequency independence and is often used to design these antennas is that of 'self-complementary antennas'. For a planar radiating structure, the complementary antenna is the one that results from replacing the conductor with vacuum and vice versa, so that if the two structures are superimposed, a continuous conducting sheet is obtained. An example is a flat dipole and an open slot in a plane of the same length and width. The input impedances of the complementary structures are in accordance with the Babinet's principle:

$$Z_{in} \cdot Z_{inComp} = \frac{Z_0^2}{4}$$

(Equation 1)

A structure is self-complementary when it and its complementary have the same shape. In this case, the input impedance is independent of frequency, and has a theoretical value of:

$$Z_{in} \cdot Z_{inComp} = \frac{Z_0}{2} = 60\pi \ \Omega \approx 188 \ \Omega$$
(Equation 2)

The simplest way to obtain a self-complementary structure is by successively rotating the equiangular element on its own axis, creating copies, or pairs of "arms" of the same shape, but rotated 180⁰.

2.1.1. Self-scalable structures

Assuming a structure defined in spherical coordinates by $r = F(\theta, \phi)$, with the excitation point located at $r = 0$, $\theta = 0$, $\phi = \pi$. This structure will be self-scaling if, subjected to a scaling factor K $[r' = K \cdot F(\theta, \phi)]$, an identical structure to r is obtained, letting it only rotate around the ϕ coordinate (Balanis, 2015). That is:

$$K \cdot F(\theta, \phi) = F(\theta, \phi + C)$$
(Equation 3)

It should be noted that C (which is only a function of K) also represents the angle that the diagram rotates for frequency $f_k = f/k$, with respect to the position it occupies for frequency f. To obtain $F(\theta, \phi)$, it suffices to calculate the derivative the two members of the equation with respect to C and ϕ:

$$\frac{d}{dC}[K \cdot F(\theta, \phi)] = \frac{dK}{dC}[F(\theta, \phi)] = \frac{\partial}{\partial C}[F(\theta, \phi + C)] = \frac{\partial}{\partial(\phi + C)}[F(\theta, \phi + C)]$$
(Equation 4)

$$\frac{d}{d\phi}[K \cdot F(\theta, \phi)] = K \cdot \left[\frac{\partial F(\theta, \phi)}{\partial \phi}\right] = \frac{\partial}{\partial \phi}[F(\theta, \phi + C)] = \frac{\partial}{\partial(\phi + C)}[F(\theta, \phi + C)]$$
(Equation 5)

Equalizing the last two terms we obtain:

$$\frac{dK}{dC}[F(\theta, \phi)] = K \cdot \left[\frac{\partial F(\theta, \phi)}{\partial \phi}\right]$$
(Equation 6)

$$\frac{1}{K}\frac{dK}{dC} = \frac{1}{F(\theta, \phi)}\frac{\partial F(\theta, \phi)}{\partial \phi} = \frac{1}{r}\frac{\partial r}{\partial \phi} \triangleq a$$
(Equation 7)

Finally, solving the differential equation in partial derivatives we obtain:

$$r = e^{a\phi}f(\theta)$$
(Equation 8)

With $f(\theta)$ being an arbitrary function. This represents an equiangular spiral represented on the surface $f(\theta)$.

2.2. Scientific bibliography review

Once the basic operation of this type of antenna was analyzed, the next step was to review previous work by authors published in the form of scientific articles specialized in equiangular spiral antennas. For this purpose, 10 journal articles were reviewed in which different application cases and improvements proposed by the authors are described.

The first article (Sirbu, Tekin, & Pouhè, 2014) begins with a detailed general theoretical description of equiangular spiral antennas. First, the authors analyzed the influence of the growth rate *a* on the shape of the radiation pattern and its directivity. They determined that, at least theoretically, the lower the rate of increase, the more directive the antenna will be.

Next, the authors analyzed the well-known geometry of equiangular spiral antennas: the generating curves and the calculation of the length of their arms. They analytically concluded that the optimal number of turns for the spiral is around 1.5. The authors also discuss the feeding structure and impedance matching methods. They proposed a tapered balun structure that allows to efficiently transform a 50Ω microstrip transmission line to a $60\pi\,\Omega$ (about 188Ω) balanced slotted line (the characteristic impedance of the antenna) as seen in *Figure 2*. They conducted the characterization of the balun from the minimum operating frequency of the antenna which defines the system.
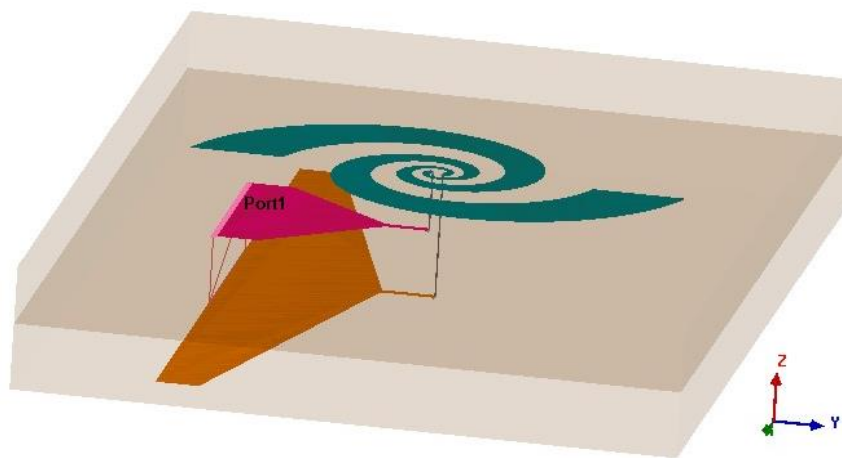
Figure 2: Antenna and tapered balun (Sirbu, Tekin, & Pouhè, 2014)

Similarly, other theorical analysis can be performed on the antennas. For example, authors (Tavakoli, Fard, & Moini, 1996) used the multiport networks analysis to determine the voltage values at each point of the patch. They segmented the antenna arms into annular segments, from which they calculated the impedance matrix using the Green function that describes each segment. Once the authors theoretically characterized the antenna, they conducted tests with a real microstrip antenna designed in the 15GHz band, for which they measured the radiation patterns of the E and H planes (*Figure 3*). From this, they found a good correlation between the previous calculations and theoretical values and the experimental ones, demonstrating the obtaining of a circular polarization for a wide range of frequencies.

6
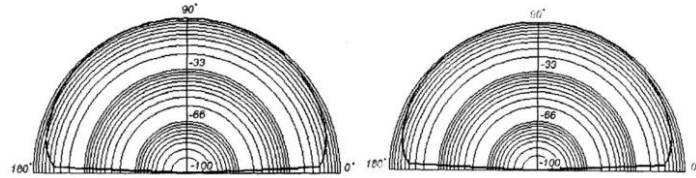
Figure 3: Measured E (left) and H (right) planes diagrams (Tavakoli, Fard, & Moini, 1996)

While microstrip antennas have a unidirectional radiation pattern, conventional spiral antennas have a bidirectional radiation perpendicular to the antenna plane. Normally, unidirectional radiation is desired, so reflecting planes or resonant cavities are used. Authors (Nakano, Kikkawa, Iitsuka, & Yamauchi, 2008) explain the use of extremely shallow resonant cavities to generate a unidirectional radiation pattern in equiangular spiral antennas. The authors used a cavity with a depth of 7mm, which is equivalent to 0.07 times the minimum wavelength for the antenna under study, 3GHz. Subsequently, the authors compared how the performance varied with the empty cavity and with filling it with a ring-shaped absorbent strip (R-ABS) and with two arc-shaped absorbent strips (A-ABSs), as detailed in *Figure 4*.
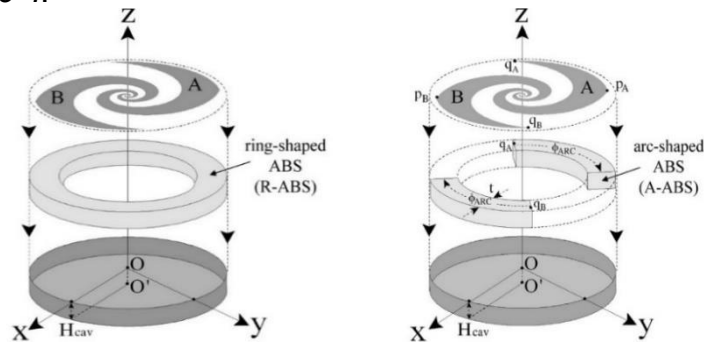
Figure 4: Ring and arc shaped absorbent to be placed inside the cavity (Nakano, Kikkawa, Iitsuka, & Yamauchi, 2008)

From the results obtained, the authors observed degradation both in the antenna's input impedance and the axial ratio when using a cavity without any absorbing material. The input impedance plot shows high ripples at low frequencies, which slowly converge to the expected value without the presence of the material. The axial ratio also has a peak of 18dB around 5.5GHz and remains above the 2dB that defines the bandwidth of equiangular spiral antennas for frequencies below 7GHz.

With the use of R-ABS, the authors obtained very constant input impedances in the range of operating frequencies. They also noted the stability of the axial ratio throughout the design frequency band below 2dB, in a remarkably analogous way to if the antenna was emitting in in free space without any cavity backing it. On the other hand, the A-ABSs (which we can interpret as a truncated R-ABS) presented more ripples in the input impedance at low frequencies, but with a low relative error compared to the expected value. The axial ratio also remained below 2dB for the entire working band. The use of two A-ABSs instead of one R-ABS has the advantage of reducing the weight of the structure, partially sacrificing the excellent input impedance stability of the complete ring. Simulations demonstrated that the gain of the antennas remained stable at around 7.1 ± 1.4 dBi, both in the presence of R-ABS and with the use of two A-ABSs within the operating band.

7

Other authors have focused on improvements for this type of antenna. A frequently occurring case is the use of parasitic elements which, when applied in a specific way, generate benefits to the antenna's operation. One case study is given by the authors (Fu, Lopez, Rowe, & Rowe, 2010), who in their article detail the inherent drawbacks of cavity equiangular spiral antennas filled with absorbent material, such as the added weight and bulk to the structure. Applications like aeronautics with these characteristics present a clear challenge that the authors seek to solve. To do this, they propose using planar antennas with built-in chip resistors or SMDs, eliminating the resonant cavity, as seen in *Figure 5*. This addition allows the design of exceedingly small antennas, by sacrificing their gain.
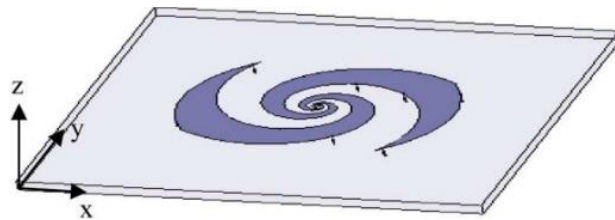
Figure 5: Proposed antenna with embedded SMD resistors (Fu, Lopez, Rowe, & Rowe, 2010)

The objective of the article is to design an antenna that operates in the frequency band from 2GHz to 18GHz and that complies with the mentioned characteristics. To do this, the authors mention the use of twelve SMD resistors connecting the edges of the spiral arms to the ground plane. The authors explain that standing waves occur at the edges of the arm circumferences and that without the use of additional components, these waves are unavoidable at certain frequencies. The resistors, which behave as pure resistances at low frequencies, absorb part of the current flowing through the antenna and ensure that it remains at low levels at the edges of the antenna at the mentioned frequencies, where its effects are most evident. This improves the bandwidth of the antenna as can be seen in *Figure 6*, along with improvements in its circular polarization.
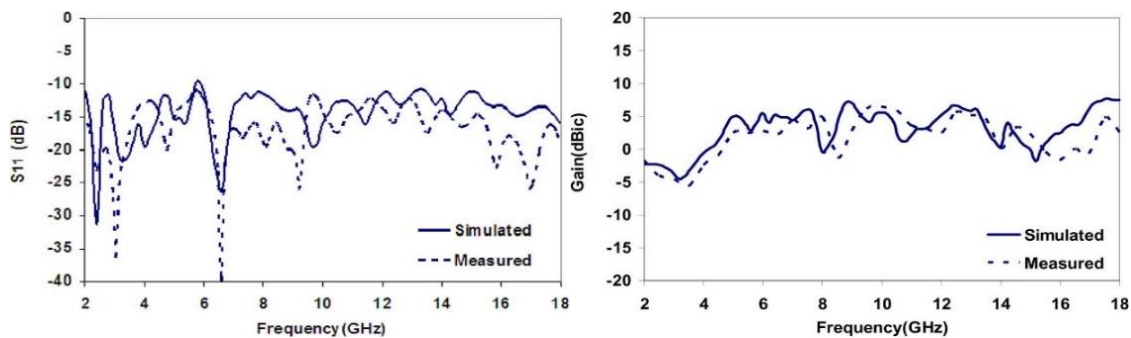
Figure 6: S_{11} parameter and gain vs frequency of the proposed antennas (Fu, Lopez, Rowe, & Rowe, 2010)

Once the authors defined the system fully, they conducted tests with both simulations and with an antenna built in the laboratory. The tests show good similarity between the simulated and the real antenna, with greater discrepancies at higher frequencies, where the reactive components of the SMDs have greater influence. The gain has values below 0dBic for frequencies in the range from 2GHz to 5GHz, due to the dissipation of energy in the resistors and between 15GHz and 17GHz, due to the appearance of surface waves. The authors note that the antenna maintained a gain over 0dBic in the rest of the band of interest.

Other types of parasitic elements different from the above are described in another article (Veysi & Kamyab, 2011). The authors analyze the possibility of using parasitic post elements together with equiangular spiral antennas, with the aim of reducing their physical dimensions and increasing the bandwidth in which they can operate. Additionally, the authors mention that this method has low costs compared to other techniques that seek similar objectives, such as the use of absorbent materials or low-profile spiral mode microstrip antennas (SMM).
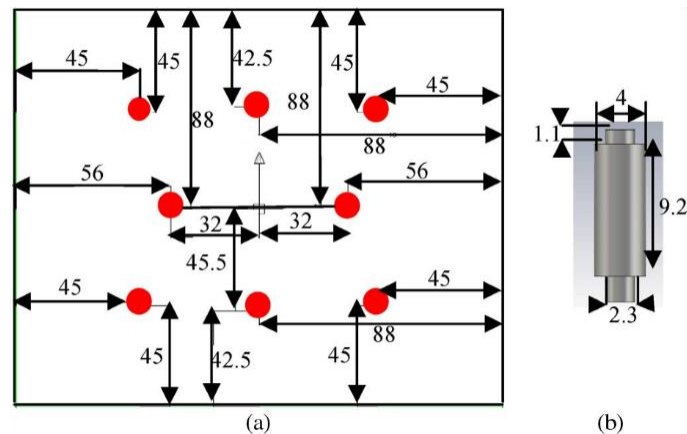
Figure 7: Proposed parasitic posts placement (Veysi & Kamyab, 2011)

The suggested parasitic elements are poles placed in such a way that they support the substrate on which the antenna rests. For the analysis, eight metal and foam posts located in the same position and compared at different heights (*Figure 7*). It was determined through simulations that the former have the advantage of significantly improving the axial ratio of the antenna and, therefore, improve circular polarization throughout the frequency band, something highly desirable in frequency independent antennas. Another advantage of metal posts is the robustness they add to the structure compared to foam posts. On the other hand, the incorporation of parasitic elements did not significantly affect other parameters such as the gain and efficiency of the antenna.

Finally, the authors made measurements from the physically created antenna, using eight 10mm-high poles and the feeding network based in a spiral-shaped microstrip transmission line. The tests showed results close enough to the simulated ones that justify the previous analysis of the authors, expressed in gain and axial ratio data presented over the frequency band. They also highlighted the antenna's broadside direction radiation pattern, with a stability evidenced for a frequency range of 6GHz.

Parasitic elements can not only improve bandwidth or reduce antenna dimensions but can also be used as frequency filters. The article (Jeon, Chang, & Pham, 2014) deals with the creation of an equiangular spiral antenna designed to have a notch band. In this case, the authors obtained this rejection band with the application of a resonant structure coupled to the antenna, although other methods to filter in the frequency domain exist. The main reason for using notch filters proposed by the authors is that frequency-independent antennas, by covering a wide range of the electromagnetic spectrum relative to the central frequency, are especially susceptible to interfering signals from external sources. In this case, the authors filtered the 5GHz ISM band.

9

The authors designed a resonant structure as a partial spiral parallel to the main spiral. The length of the partial spirals and their location control the center frequency and the width of the stop band. For the experimental design, they used a spiral identical to the main one at the back of the antenna and a pair of vias to connect the feed point to the desired point on the main spiral. The vias work as a balun, electrically reducing the spiral. This design can be seen in *Figure 8*.

Figure 8: Constructed antenna and balun system (Jeon, Chang, & Pham, 2014)

For this purpose, the authors defined an antenna with the same parameters and then proceeded to simulate it. They compared the results with the measured ones and with another simulation without the resonant element. The gain showed values of around 5dBi for the pass band and -12.5dBi for the stop band, as seen in *Figure 9*. It is important to highlight that the real antenna presented a shift in the central frequency of the stop band, due to errors in the manufacturing process, which the authors expect to improve in future revisions.
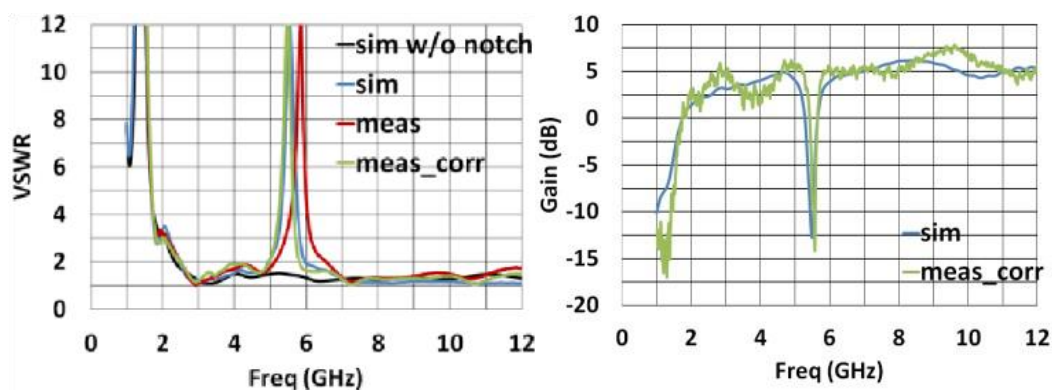
Figure 9: VSWR and gain vs frequency plots showing the generated notch (Jeon, Chang, & Pham, 2014)

Another type of parasitic elements under study are dielectric lenses. Another article (Garufo, Llombart, & Neto, 2016) is based on the application of these lenses applied to equiangular spiral antennas (*Figure 10*). The authors postulate that when feeding a dense dielectric lens with a frequency-independent antenna, the property of constant input impedance remains, but the lens itself affects the radiation pattern. That is the reason the authors focus on finding solutions to maintain a minimum dispersion. As is known, equiangular spiral antennas present equal radiation in the two directions perpendicular to itself. Achieving directivity requires either the use reflecting planes that limit the bandwidth or inserting an absorbing dielectric in a resonant cavity below the antenna.

10
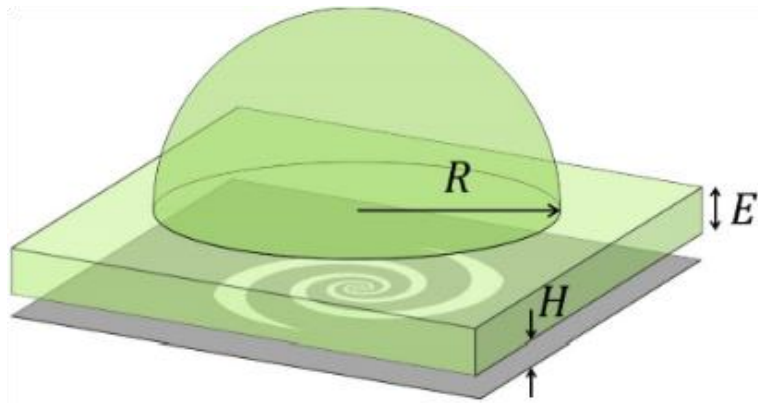
Figure 10: Equiangular spiral antenna with a dielectric lens (Garufo, Llombart, & Neto, 2016)

As a first test, the authors simulated the antenna at an infinite air-dielectric interface, an approximation to the dielectric lens. The authors evaluated different spirals at various frequencies (10GHz, 30GHz and 50GHz) and after trial and error, it is shown that a larger beamwidth was obtained with an antenna generated with a growth rate $a \approx 1.34$ and $\delta = 150°$ in the generating equation of the arms. This means that the antenna is no longer self-complementary under normal conditions (which, according to theory, implies that $\delta = 90°$), but in the presence of the dielectric, it presents better values. The authors defined as this structure as the "optimized antenna." This structure presents a notable improvement both in the gain of the antenna and in its axial ratio with respect to the conventional spiral.

Subsequently, the authors analyzed the possibility of improving the gain of the system by adding a separation (film of air) between the dielectric and the antenna's body. For the separation to be useful, the authors mention values of $H \leq \lambda_0/10$. However, the optimum values vary not only with the operating frequencies, but also with the shape of the chosen spiral. The authors maintain that for a spiral with $\delta = 45°$, an optimal value of $\lambda_0/15$ is desired.

For the feeding structure, authors concluded that for millimeter waves the only feasible alternative is to use a microstrip transmission line. However, the width of the substrate presents a challenge because it depends on the frequency, being necessary to use substrates tens of micrometers wide for higher frequencies. Given the difficulty of reaching such widths in practice, it is normal to use wider substrates. The main consequence of that is the appearance of imbalances in the structure that are likely to affect the operation primarily at lower frequencies.

To study the influence of the lens, authors constructed a silicon one mounted over an equiangular spiral antenna. The lens caused an increase in the directivity of the system, evident in the radiation patterns and at all frequencies, compared to the antenna without lens. The lens also helps reduce the scatter inherent in all spiral antennas since the radiation occurs from different sections of the spiral at different frequencies. In conclusion, the authors highlight the design of a printed spiral between the dielectric and air interface and coupled to a synthesized elliptical lens to achieve high beamwidth efficiency at wide bandwidths. Additionally, the lens improves the directivity of the system remarkably, as seen in *Figure 11*.
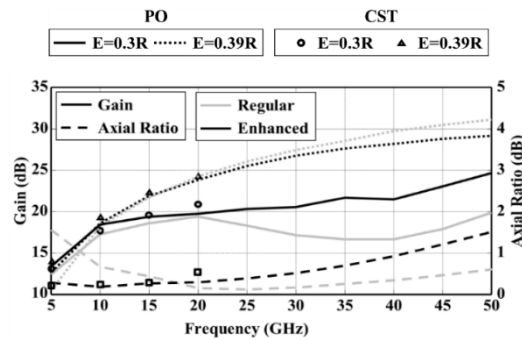
11

Figure 11: Improvement of the parameters of the system (Garufo, Llombart, & Neto, 2016)

One area where studies are also being conducted to improve the performance of this type of antenna is in its physical form. Authors from one article (Sugak, Ballandovich, Kostikov, Antonov, & Liubina, 2018) seek to miniaturize equiangular spiral antennas while maintaining their main characteristics of frequency independence and circular polarization in the working bandwidth. A technique described by the authors to miniaturize the antenna is with the use of "cogged" and non-uniform structures they studied so far, like those of *Figure 12*. This expands the outer surface of the antenna which surface currents traverse.
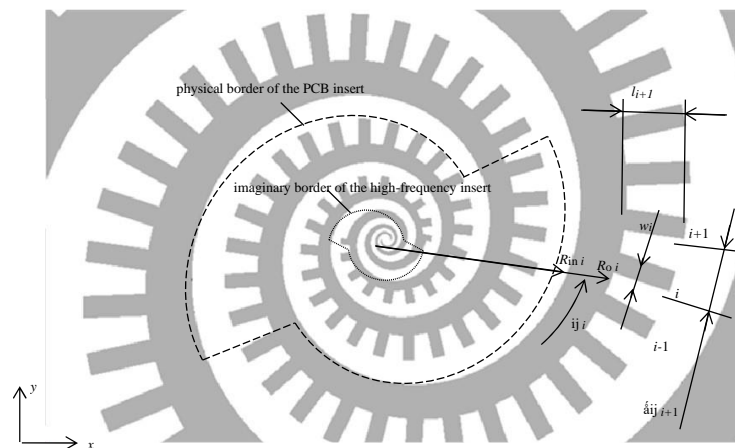
Figure 12: Proposed "cogged" spiral antenna (Sugak, Ballandovich, Kostikov, Antonov, & Liubina, 2018)

The authors used a high-frequency PCB insert in the center of the antenna. This element resonates at higher frequencies that the antenna, so they expected to make it possible to expand the bandwidth to the desired range with its use. Subsequently, the authors described the equations that define the geometry of the antenna thoroughly, and then used them to create a proposed design. The antenna was designed to have a characteristic impedance of 100Ω. This means that they had to use a 50Ω to 100Ω converter to match the impedance the antenna.

Finally, the authors conducted both simulated and physical tests of the antenna, which demonstrated the correct analysis they made and the fulfillment of obtaining a greater operating bandwidth with the use of the high-frequency PCB component. It is necessary to highlight that the authors empirically found the need to use absorbent material to compensate for the asymmetric currents caused by the unbalanced feeding method used. The authors proposed to design a new balanced feeding network in future designs.

In the field of applications of this type of antenna, there are different examples of current use. One of them (García Martínez, Sánchez Olivares, Fernández González, & Tamayo Domínguez, 2022) deals with an application case for equiangular spiral antennas in an antenna array for mounting on space launcher fuselages. For this purpose, the antennas must operate in the S band. To achieve this, the authors designed an array to provide the geographic coverage needed by the launcher. The idea of using an equiangular spiral antenna instead of the helix antennas commonly used for these applications arises from the need to provide circular polarizations for higher bandwidths, something that helix antennas are not capable of achieving, plus re desired reduced dimensions that the spiral antennas provide.
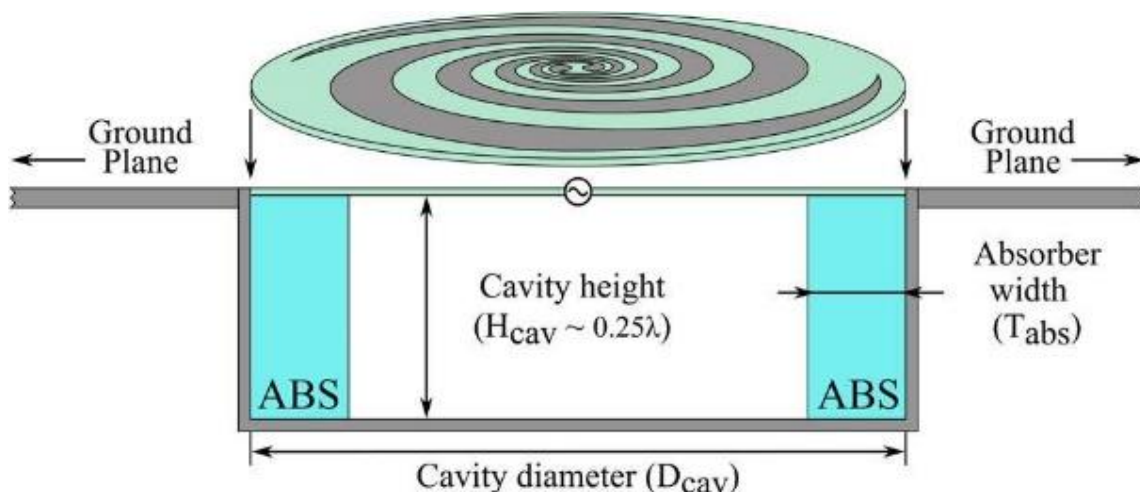
Figure 13: Proposed antenna assembly to be mounted in the fuselage (García Martínez, Sánchez Olivares, Fernández González, & Tamayo Domínguez, 2022)

In this sense, the authors designed the antenna following the theoretical bases already known for equiangular spiral antennas: two arms displaced 180° and created from a generating function rotated about the center. The design of the antenna includes a cavity with a depth of $\lambda/4$ of the lowest frequency of interest (2GHz). Inside the cavity, authors introduced a ring-shaped absorbing material (R-ABS) to achieve unidirectional radiation. As an impedance transformer, the balun they designed is an exponential tapered one, which allows transforming the $60\pi\,\Omega$ input of the antenna to a 50Ω coaxial line. The proposed design can be seen in *Figure 13*.

To verify the approach, authors physically built an antenna with all the characteristics proposed (*Figure 14*) and a performed a simulation with the same parameters. They conducted a study in a frequency band between 2GHz and 3.4GHz, the band where the antenna should theoretically be able to operate following the circular polarization requirement. In both cases, the authors obtained an S_{11} parameter well below -10dB for the entire frequency range under study. As for the axial ratio, they observed a discrepancy between the simulation and the manufactured antenna, where peaks above 2dB appear for frequencies below 2.1GHz and between 2.9 and 3.2GHz. The authors attribute these differences to manufacturing errors. The results showed antenna efficiency values above 75%.
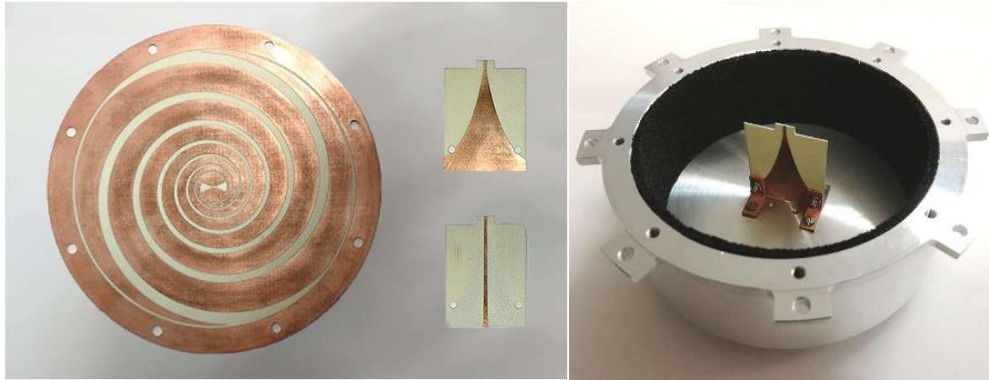
Figure 14: Antenna and balun for aerospace applications (García Martínez, Sánchez Olivares, Fernández González, & Tamayo Domínguez, 2022)

Another use case for these antennas can be in radar applications. One article (Sakomura, Ferreira, Bianchi, & Nascimento, 2018) describes a combined spiral antenna with unidirectional radiation in the 1GHz to 11GHz band to be used in a direction finding (DF) system. The article details the feeding system of the antenna designed with a tapered balun to operate in the mentioned band.

The authors designed the antenna with easily available commercial elements and, as a novelty, the design combines an Archimedean spiral in the inner area with a well-known equiangular spiral in the outer region. The Archimedean spiral serves as a microstrip transmission line for the equiangular spiral. Authors placed the antenna over a resonant cavity which generates unidirectional radiation. This cavity was filled with absorbing material to ensure frequency-independent behavior in a single radiation direction. Finally, they terminated the arms of the system with a 130Ω resistor connected to the walls of the cavity. This design, shown in *Figure 15*, combines different elements previously found in the previously reviewed articles by (Fu, Lopez, Rowe, & Rowe, 2010) and (Nakano, Kikkawa, Iitsuka, & Yamauchi, 2008).

Fig.1. Geometry of the proposed compound spiral antenna simulated in HFSS.

Figure 15: Radiating spiral antenna and its feeding network (Sakomura, Ferreira, Bianchi, & Nascimento, 2018)

14

For feeding and impedance matching, authors used a tapered balun, composed of a microstrip line that gradually transforms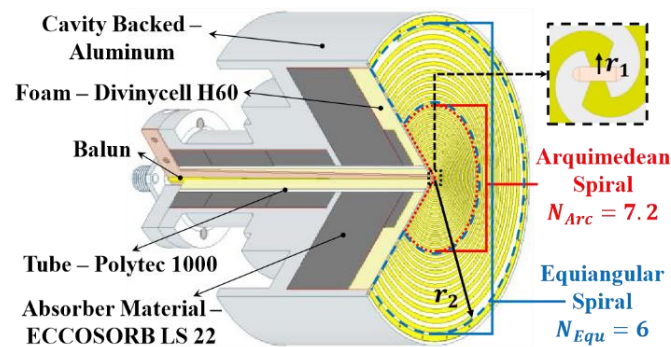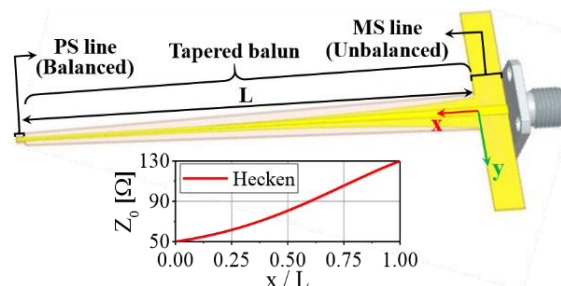 into a line of parallel strips, transforming the line from unbalanced to balanced and matching the impedances in the process. The creation of the balun uses the Hecken spiral to define the shapes of the transmission lines.

At this point, the authors analyzed the constructed prototype and determined it to be adequate to operate in the frequency band under study. They obtained a reflection coefficient of less than -9.5dB and an axial ratio of less than 3dB in the entire operating band. The radiation patterns present a clear unidirectional radiation with wide beam openings, between 115.5º and 159.5º in the mentioned band. Another remarkable feature presented by the prototype is the great symmetry in the radiation patterns In the H and E planes, as seen in *Figure 16*.

Lastly, the authors evaluated the antenna for the direction search application and presented absolute error values that were always under 3º, the limit originally set by them to validate the antenna. These results confirm that the DF system based on the compound antenna can estimate the angle of arrival (AoA) of electromagnetic signals with the precision needed.
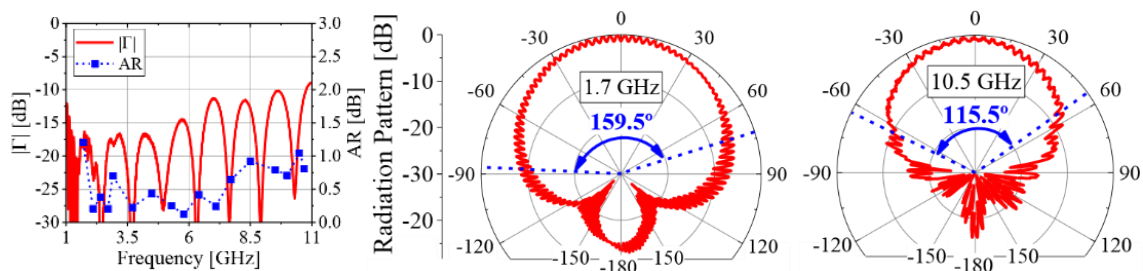
Figure 16: Reflection coefficient and radiation diagrams for the DF system (Sakomura, Ferreira, Bianchi, & Nascimento, 2018)

Given the large amount of scientific material available in leading scientific publications, the interest in developing this type of antenna and its current applications is evident. Therefore, it is necessary to have a method to simulate these antennas in the simplest feasible way and to obtain results that show all the desired parameters of interest.

2.3. Design parameters analysis

As explained by (Anguera & Pérez, 2008), when the self-scaling structure equation analyzed in section 2.1.1 is drawn on a plane of constant $f(\theta) = R_0$, the following equation is obtained, representing a planar equiangular spiral, from which the arms of the antenna can be constructed.

$$r = R_0 e^{a\phi}$$
(Equation 9)

Both the literature and MATLAB itself define different parameters (*Figure 17*) of interest that engage in the creation of these antennas and that will be necessary to understand before performing any type of simulation of this type of antennas.

15

- **Inner radius:** the inner radius of the antenna is measured from the center of the structure to the center of the first turn. This parameter represents the R_0 in the generating equation and determines the maximum operating frequency of the antenna as follows:

$$R_0 = \frac{c_0}{2\pi f_{hi}}$$
(Equation 10)

- **Outer radius:** the outer radius is measured from center of the spiral to center of the outermost turn. This parameter determines the minimum operating frequency of the antenna as follows:

$$R_{max} = \frac{c_0}{2\pi f_{low}}$$
(Equation 11)

- **Growth rate and number of turns:** the growth rate, also known as the flare rate or winding angle, represented as a in the generator equation, can be seen as a measure of how much the antenna wraps around itself. It seems clear that if an antenna wraps more around itself, its arms will have more turns. The relationship between the angular displacement ϕ and the number of turns can be rewritten as:

$$\phi = 2\pi N$$
(Equation 12)

Substituting in the main equation, we obtain:

$$r = R_0 e^{a2\pi N}$$
(Equation 13)

$$a \cdot N = \frac{1}{2\pi} \ln\left(\frac{r}{R_0}\right)$$
(Equation 14)

From here, it becomes clear that the product $a \cdot N$ is logarithmically proportional to the quotient r/R_0. The value R_0 is a design parameter that sets the highest operating frequency. On the other hand, the position in the r plane depends on the relative number of turns the spiral travels. The tip of each arm is reached when there has been an angular displacement of $2\pi N$ turns or, equivalently, the exact number of turns that each arm has moved. Unfortunately, the number of turns is not related to any of the design parameters for this type of antenna.
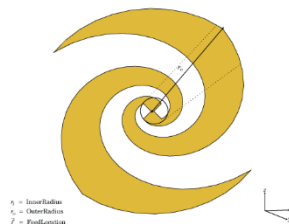

Figure 17: Design parameters of the equiangular spiral antennas in MATLAB

However, since the outer radius is measured to the center of the last turn, it can be used to help estimate this parameter from a given growth rate:

$$N \gtrapprox \frac{1}{2\pi a} \ln\left(\frac{R_{max}}{R_0}\right)$$
(Equation 15)

The actual number of turns will always be strictly greater than the calculated one due to the inaccuracy presented by the radial point at which the calculation is made. However, this difference will be small and can be used as a good approximation. Similarly, the growth rate can be adjusted so that the antenna has a *minimum* number of turns using the same expression. *Figure 18* shows different antennas generated with the same frequency parameters ($f_{low} = 1GHz$, $f_{hi} = 6GHz$) and different growth rates calculated from the above expression based on a preset number of turns. The antennas have the same physical width (about 100mm).

| N≈0.5 turns | N≈1 turn | N≈2 turns |
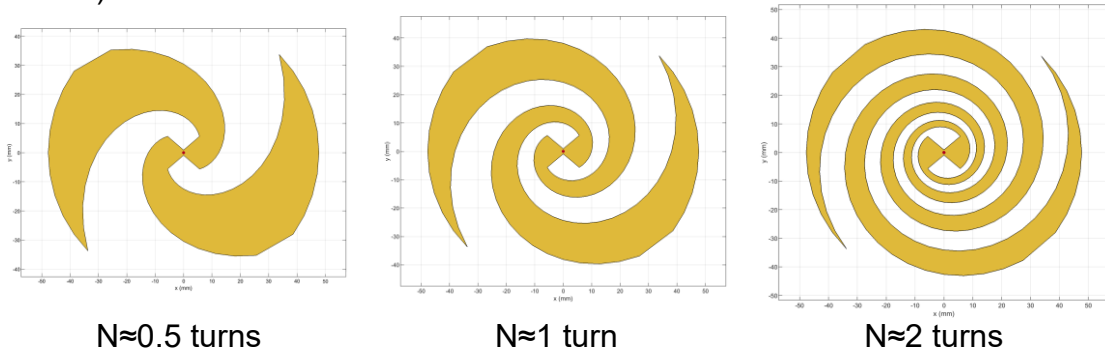
Figure 18: Antennas generated using different growth rates from a given number of turns

2.4. Description of the simulation process

The simulations were executed MATLAB using the built-in Antenna Toolbox. This toolbox includes a command to generate equiangular antenna objects, *spiralEquiangular*. Once the antenna has been created, different properties can be set on the antenna:

- **GrowthRate:** the equiangular spiral growth rate. The default value is 0.35.
- **InnerRadius:** inner radius of the spiral. The default value is 0.002.
- **OuterRadius:** outer radius of spiral. The default value is 0.0189.
- **WindingDirection:** defines the direction of the spiral turns. The options are 'CW' (clockwise) and 'CCW' (counterclockwise). This parameter can change the circular polarization direction. The default direction is 'CCW'.
- **Conductor:** Type of metal material. MATLAB includes a built-in catalog of metals called which can be visualized with the MetalCatalog command. The default material is a PEC.
- **Load:** defines lumped elements added to the antenna feed. The default load is an empty element.
- **Tilt:** Tilt angle of antenna. The default value is zero.
- **TiltAxis:** specifies the coordinate around which the antenna can rotate. By default, the coordinate is the X axis.

17

2.5. Parameterization and previous calculations

Before starting the simulation process as such, it is necessary to define which physical reference parameters the antenna will have. From this point on, the reference band for the antenna will be between 1GHz and 6GHz, which represents a bandwidth of more than 1.4:1. The simulations will be carried out in the frequency band from 0.5 to 8GHz and five values will be taken for the point frequency simulations: 1.2GHz, 2.5GHz, 3.5GHz, 5.8GHz and 8GHz, the latter outside the expected operating band. Frequency-dependent measurements (such as S_{11} parameter and input impedance) will be simulated with at least one hundred points of resolution.

Since the antenna is defined to operate in a certain frequency range (1-6GHz), the *InnerRadius* and *OuterRadius* parameters are to be calculated in base to this range.

$$\text{InnerRadius} = R_0 = \frac{c_0}{2\pi f_{hi}} = \frac{c_0}{2\pi \cdot 6 \cdot 10^9} = 7.95\ mm$$
(Equation 16)

$$\text{OuterRadius} = R_{max} = \frac{c_0}{2\pi f_{low}} = \frac{c_0}{2\pi \cdot 10^9} = 47.71\ mm$$
(Equation 17)

The other main parameter that can be modified is the *GrowthRate*, which will be reviewed in coming sections. The simulations will evaluate the effect of varying that parameter.

2.6. Simulations procedure

This section describes in detail the code used to generate each type of simulation described, along with a brief explanation of how each code works and what it is expected to generate as its output. The results generated by the code are shown below, in each corresponding subsection.

The MATLAB antenna toolbox works with "antenna" format objects. The first step before performing any simulation will then be to create the antenna object itself. In this case, the antenna object will be arbitrarily named *spiralAnt*. The parameters calculated in the previous section are also set to the antenna using the following code:

```
%Create the equiangular spiral antenna object
spiralAnt=spiralEquiangular;
spiralAnt.InnerRadius=0.00795;
spiralAnt.OuterRadius=0.04771;
```
Figure 19: Code to create the equiangular spiral antenna object

The code creates the antenna object spiralAnt and assigns it the InnerRadius and OuterRadius properties, obtained analytically in the section *2.5*. The first simulation was carried using the default growth rate of 0.35. This represents slightly over 0.8 turns. The material is also left as the default PEC. The generated object can be seen in
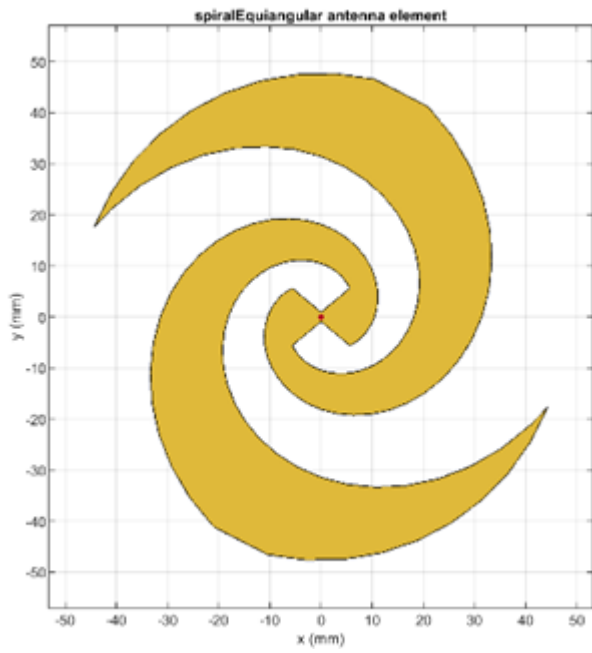
Figure 20.
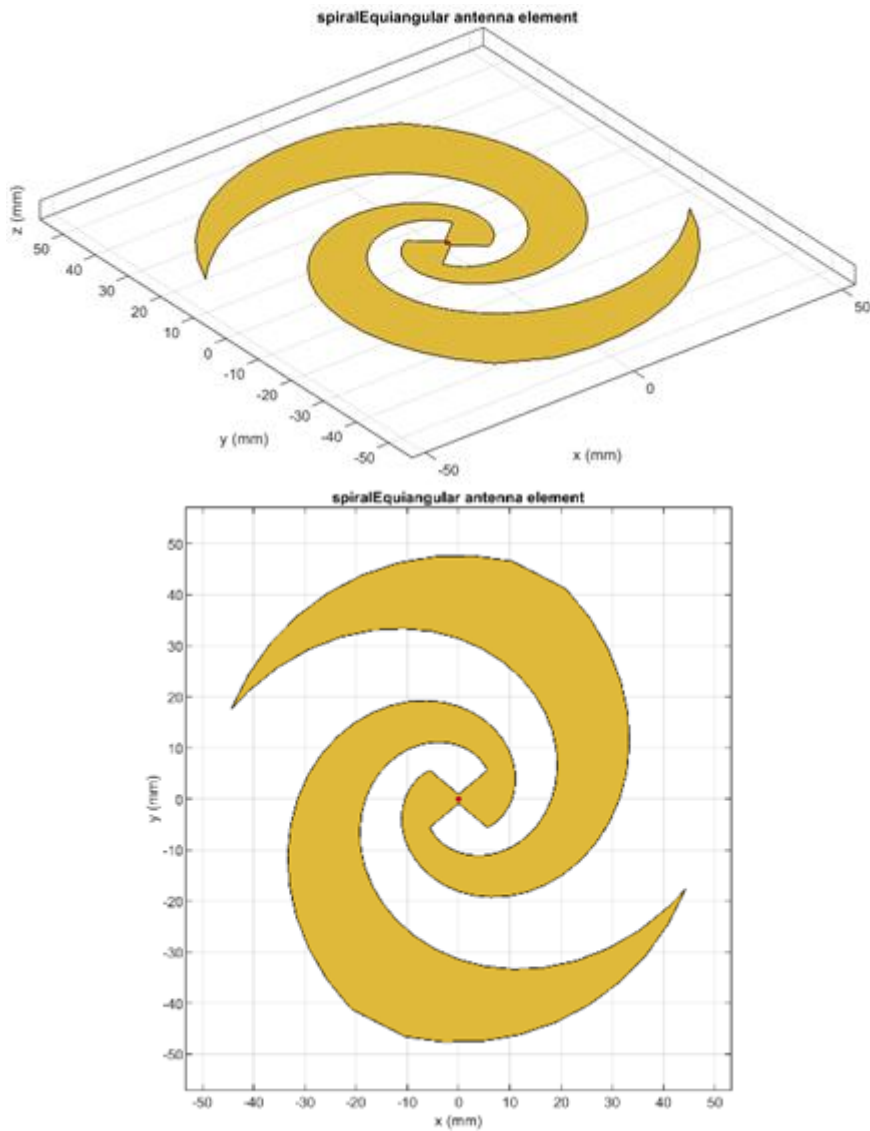
Figure 20: Generated antenna with the default 0.35 growth rate

19

To facilitate the comparison of the results obtained, an equal dynamic range has been defined for all the simulations of the same type. Thus, for the 2D radiation patterns, a range of gain magnitudes between -20 and 10 dBi was set in "Magnitude Axis" property box, as shown in the *Figure 21*.
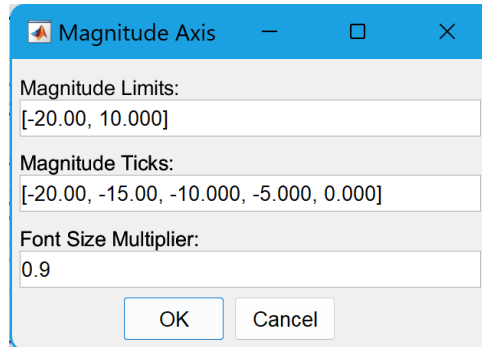
Figure 21: Magnitude properties used for all the 2D diagrams simulations

For the 3D radiation patterns, the range between -10 and 10dBi was used in the "Colormap Editor" for ease of visualization, as shown in the *Figure 22*.
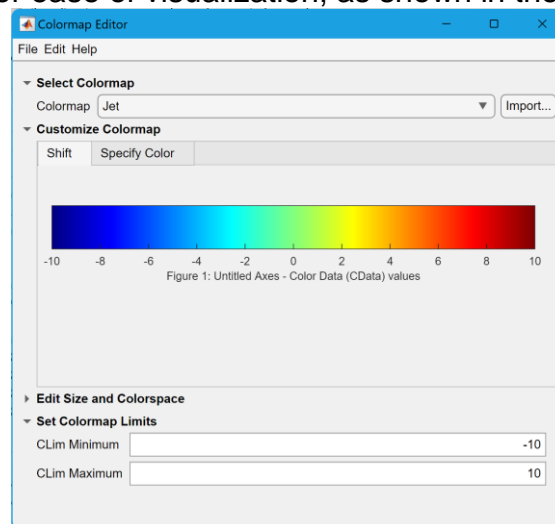
Figure 22: Colormap properties used for all the 3D diagrams simulations

Finally, for the surface currents, a range between 0 and 1A has been used in the "Colormap Editor", as shown in the *Figure 23*.
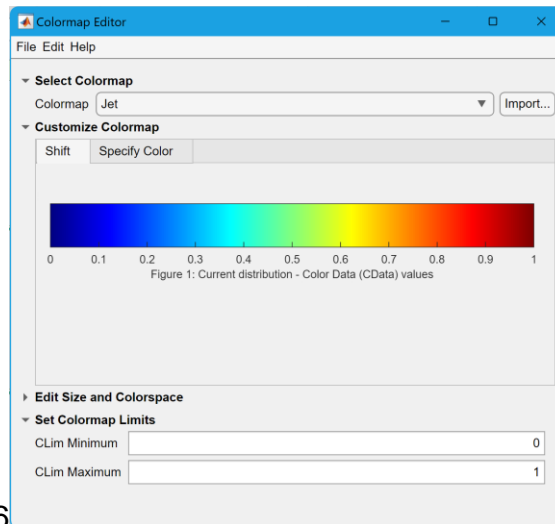
Figure 23: Colormap properties used for all the surface currents simulations

2.6.1. 2D Radiation diagrams

The first simulations to be performed are the radiation patterns (Gain) calculations. The code for obtaining the azimuth-plane patterns in the five mentioned frequencies in section 2.5 is:

```
%Generate the azimuth plane diagrams
az1=patternAzimuth(spiralAnt,1.2E9);
az2=patternAzimuth(spiralAnt,2.5E9);
az3=patternAzimuth(spiralAnt,3.5E9);
az4=patternAzimuth(spiralAnt,5.8E9);
az5=patternAzimuth(spiralAnt,8E9);
p=polarpattern([az1 az2 az3 az4 az5],'Peaks',1,'TitleTop',"Azimuth plane Gain
(dBi)");
createLabels(p,'f=%0.1fGHz',[1.2 2.5 3.5 5.8 8]);
showPeaksTable(p, 1);
```

Figure 24: Code to generate the azimuth plane diagrams
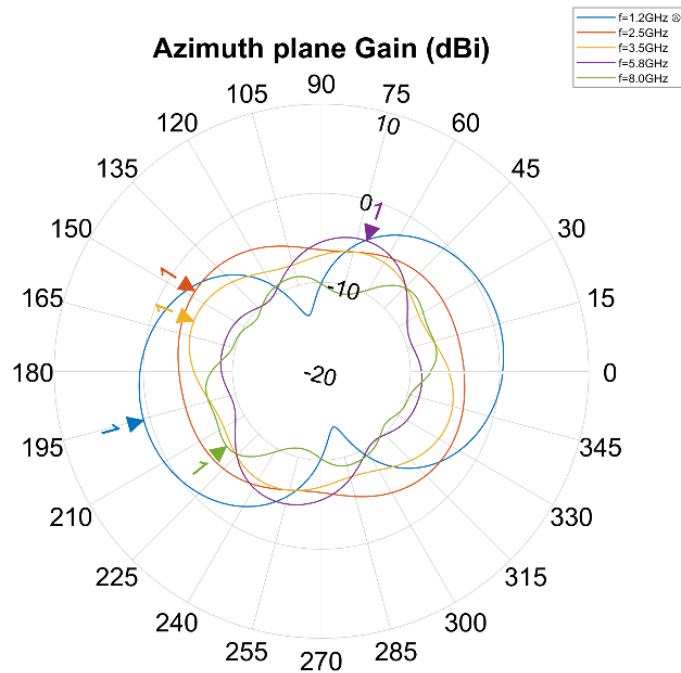
Figure 25: Azimuth plane gain for the first simulated antenna

Frequency	Degrees (⁰)	Magnitude (dBi)
1.2GHz	195.5	0.7
2.5GHz	147.6	-3.2
3.5GHz	158.6	-4.6
5.8GHz	70.8	-4.5
8GHz	218.4	-6.4

Table 1: Azimuth plane gain maximums

In this case, it is noticeable from *Figure 25* that the antenna is barely radiating power to its sides. The gain starts with a rather low value at the lowest frequency under study and decreases significantly at mid and high frequencies. Maximum values seen in *Table 1* show this behavior, stating from a value of 0.7dBi and reaching gains a low as -6.4dBi. This matches the expected behavior of planar spiral antennas.

Similarly, the elevation-plane radiation diagrams can be obtained with the following code:

```
%Generate the elevation plane diagrams
el1=patternElevation(spiralAnt,1.2E9);
el2=patternElevation(spiralAnt,2.5E9);
el3=patternElevation(spiralAnt,3.5E9);
el4=patternElevation(spiralAnt,5.8E9);
el5=patternElevation(spiralAnt,8E9);
p=polarpattern([el1 el2 el3 el4 el5] ,'Peaks',1,'TitleTop',"Elevation plane
Gain (dBi)");
createLabels(p,'f=%0.1fGHz',[1.2 2.5 3.5 5.8 8])
showPeaksTable(p, 1)
```

*Figure 26: Code to generate the elevation plane diagrams*

These lines of code use the *patternAzimuth* and *patternElevation* commands to calculate the gain in the planes in polar form. These results are stored in variables for each frequency of interest (az1/el1, az2/el2, etc...). The *polarpattern* function is used to display them superimposed on a single plot as well as showing the maximum peaks of each calculation.
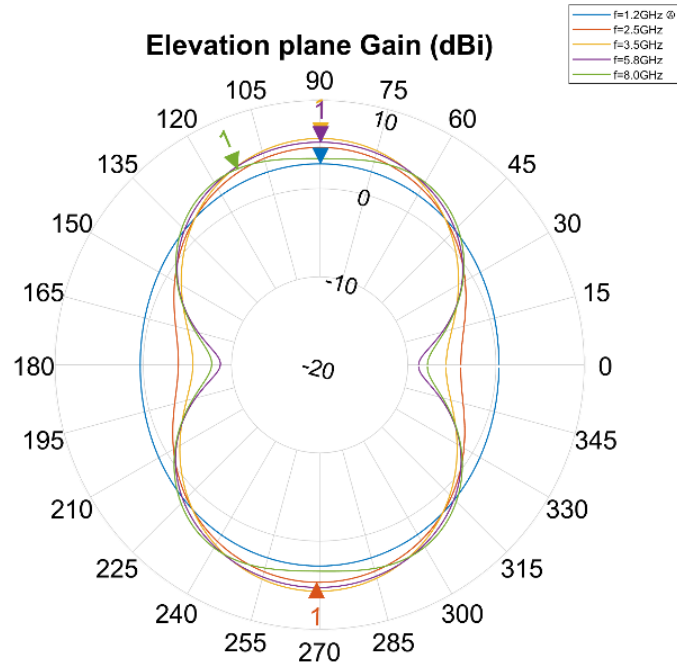
Figure 27: Elevation plane gain for the first simulated antenna

Frequency	Degrees (⁰)	Magnitude (dBi)
1.2GHz	89.8	2.8
2.5GHz	269.3	4.7
3.5GHz	89.8	5.7
5.8GHz	89.8	5.3
8GHz	112.7	4.1

Table 2: Elevation plane gain maximums

From *Figure 27* it is possible to see that the antenna displays the expected behavior, with symmetric lobes perpendicular to the antenna plane. The gain remains stable beyond the center frequency but is lower than the expected for the lower one close to the minimum operating frequency by design (*Table 2*).

2.6.2. 3D Radiation diagrams

Next, the 3D radiation diagrams are generated with these commands:

```
%Generate the 3D radiation diagrams
pattern(spiralAnt,1.2E9);
pattern(spiralAnt,2.5E9);
pattern(spiralAnt,3.5E9);
pattern(spiralAnt,5.8E9);
pattern(spiralAnt,8E9);
```

Figure 28: Generate the 3D radiation diagrams

In this case, the *pattern* command graphically generates the radiation pattern for a specific frequency. The command must be executed separately for each frequency of interest (five times, in this case), generating a graph from *Figure 29* each time a line was run.

f=1.2GHz

f=2.5GHz

f=3.5GHz

f=5.8GHz
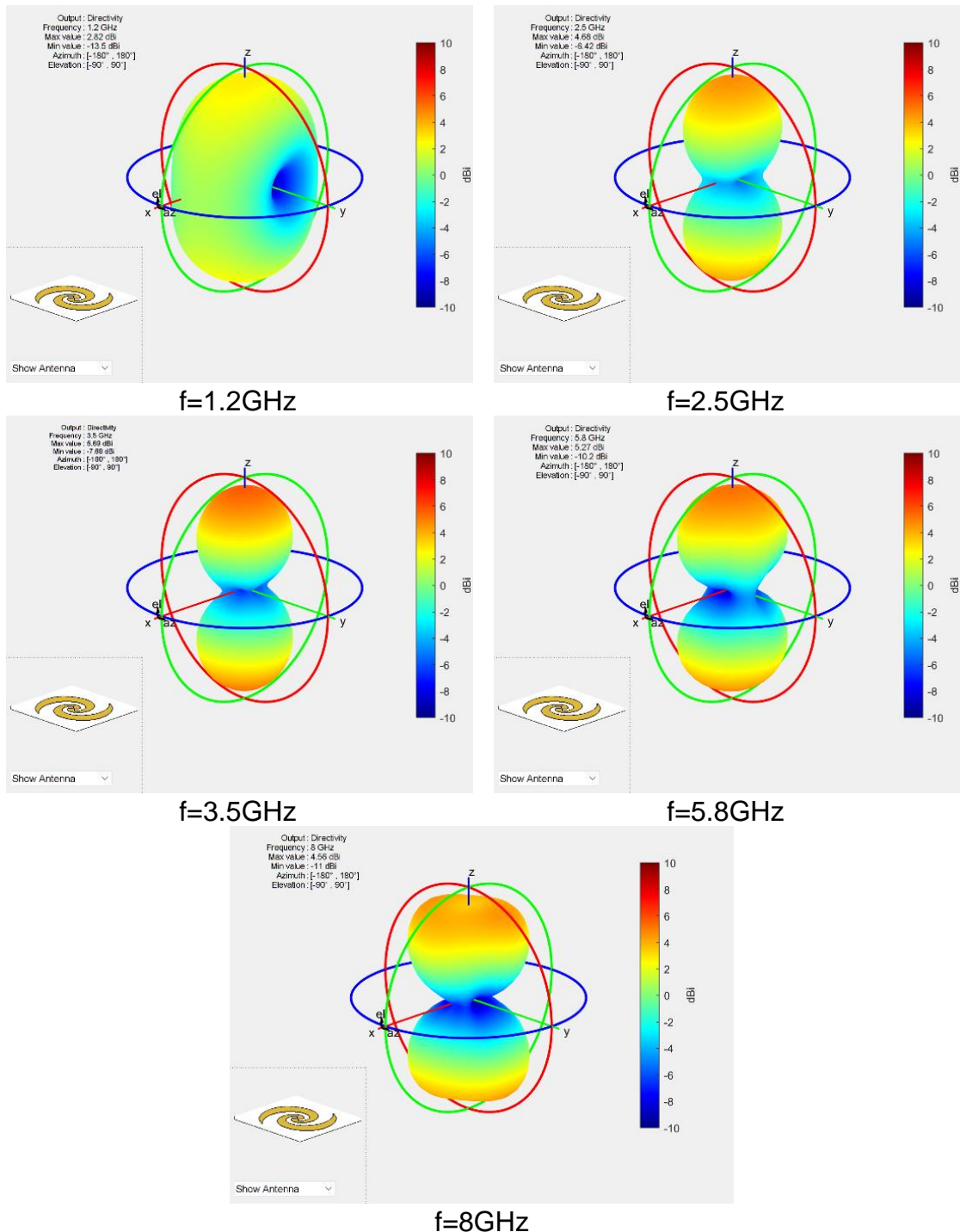

f=8GHz

Figure 29: 3D radiation diagrams for different frequencies for the first simulated antenna

The results are consistent with the planar plots obtained before and show the expected pattern for this type of antennas, especially for the higher frequencies. The lower frequency diagram shows a faint radiation (not much greater than 0dBi) in the X-axis direction, which is unexpected.

24

2.6.3. S_{11} parameter

The next specification to be simulated is the S_{11} parameter, which can help to infer the input voltage reflection coefficient of the system. The plot of the parameter versus frequency can be easily calculated with the following command:

```
%Generate the S11 parameter plot
rfplot(sparameters(spiralAnt, 0.5E9:0.05E9:8E9));
```

Figure 30: Code to generate the S11 parameter plot

The *sparameters* command generates the values of parameter S_{11} in a specified frequency range. In this case, 50MHz steps are made, which represents 151 measurement points. The *rfplot* command makes a graphical representation of the result obtained.
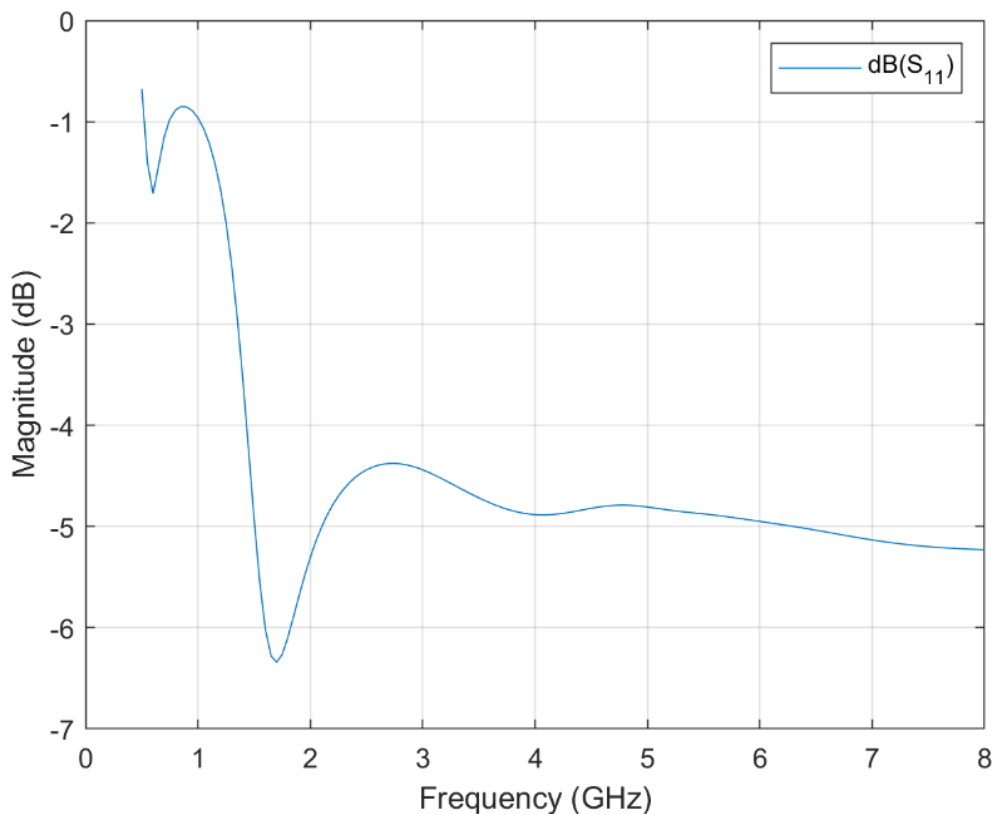
Figure 31: S_{11} parameter versus frequency for first simulated antenna

From the plot of *Figure 31* is possible to observe that the parameter remains overall constant over 2GHz frequency mark. However, between the 1-2GHz band, the parameter remains unstable, which fails to achieve the expected behavior for the operating band. This is especially noticeable from the frequencies below the 1.5GHz mark, having an elevated S_{11} parameter and, in consequence, a considerable. impedance mismatch

25

2.6.4. Input impedance

In a similar way to the previous subsection, the input impedance versus frequency plot can be easily obtained with the following command:

```
%Generate the input impedance plot
impedance(spiralAnt,0.5E9:0.05E9:8E9)
ylim([-100 250])
```

Figure 32: Code to generate the input impedance plot

The *impedance* command generates both the real and the imaginary part of the impedance as a function of the given frequency range. In this case, as in the case of parameter S_{11}, the graph is obtained at 151 points. Additionally, the limits on the ordinate axis have been adjusted to show only relevant values. A second plot has been generated detailing the absolute value of the input impedance compared to the expected value for a self-complementary structure. The command to generate such a plot is as follows:

```
%Generate the input impedance comparison plot
plot([0.5:0.05:8],abs(impedance(spiralAnt,0.5E9:0.05E9:8E9)),'LineWidth',2)
yline(60*pi,'-g','LineWidth',2)
ylabel('Impedance (\Omega)')
xlabel('Frequency (GHz)')
legend('Input impedance (absolute value)','60\pi\Omega (expected value)')
grid on
title('Comparison with the expected value')
```

Figure 33: Code to generate the input impedance comparison plot

The code again uses the *impedance* function to calculate the input impedance of the antenna and then, the absolute value is plotted. A constant value of $60\pi\,\Omega$, which is the expected input impedance for a self-complementary structure, is added to the plot with the *yline* command and displayed in *Figure 34*.
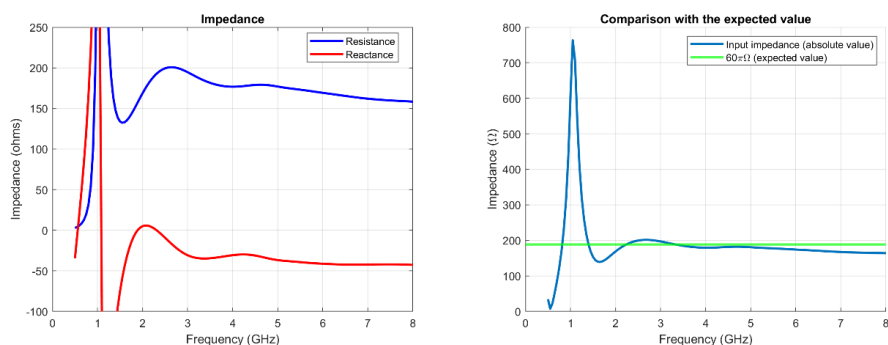
Figure 34: Input impedance versus frequency for first simulated antenna

Again, the impedance remains stable for the 2-6GHz band but does not seem to operate well for the lower frequencies of the defined range. Above the 2GHz marks, the antenna maintains an absolute value that remains close to the expected $60\pi\Omega$ for self-complementary antennas, as expected according to the theory detailed in the section 2.1. The absolute impedance starts decaying slowly from 5GHz onwards. The fact that the input impedance remains constant is a good measure to determine the frequency independence of the antenna.

2.6.5. Axial ratio

The axial ratio is the next parameter to be analyzed, which defines the quality of the circular polarization, often mentioned in the bibliography as one of the main reasons for using the equiangular spiral antennas over other types of frequency independent antennas. The axial ratio is the ratio of the magnitudes of the major and minor axis defined by the electric field vector. The following command shows the axial ratio versus frequency plot:

```
%Generate the axial ratio plot
axialRatio(spiralAnt,0.5E9:0.05E9:8E9,0,90);
ylim([0 10])
```

Figure 35: Code to generate the axial ratio plot

The *axialRatio* command generates the plot of the axial ratio as a function of frequency. As in the previous cases, the simulation is conducted for 151 frequency points. The limits of the plot for the ordinate axis have been defined between 0 and 10dB with the use of the *ylim* command, for a better visualization of the values of interest.
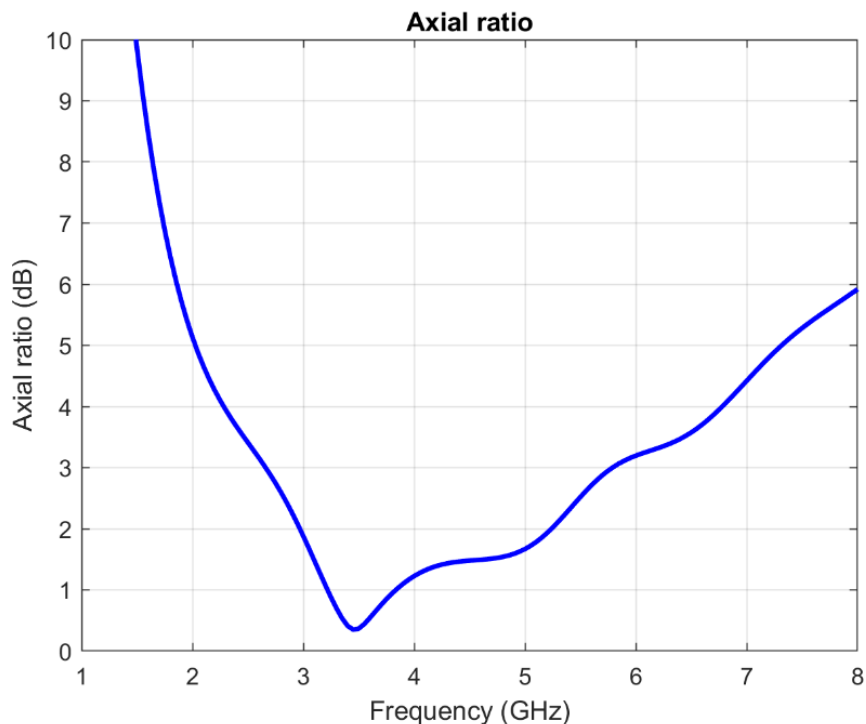
Figure 36: Axial ratio versus frequency for first simulated antenna

An acceptable circular polarization is usually considered for values of the axial ratio below 3dB. As it can be seen in the *Figure 36*, the simulated antenna displays said axial ratio in the range of 2.5-6GHz. Frequencies lower than these show an exaggerate ratio which in turn means that the polarization becomes elliptical, which can be considered undesirable as mentioned. In turn, the polarization reaches its most circular value around the center frequency (3.5GHz) as expected.

2.6.6. Surface currents distributions

Lastly, the surface currents distribution can similarly be obtained. For that, the following commands are used:

```
%Generate the current distribution graph
current(spiralAnt,1.2E9);
current(spiralAnt,2.5E9);
current(spiralAnt,3.5E9);
current(spiralAnt,5.8E9);
current(spiralAnt,8E9);
```

Figure 37: Code to generate the current distribution graph

Each execution of the *current* command shows the distribution of the currents on the antenna surface in a two dimensions plot. As the command is performed per frequency, it must be executed once for each frequency to obtain each plot.
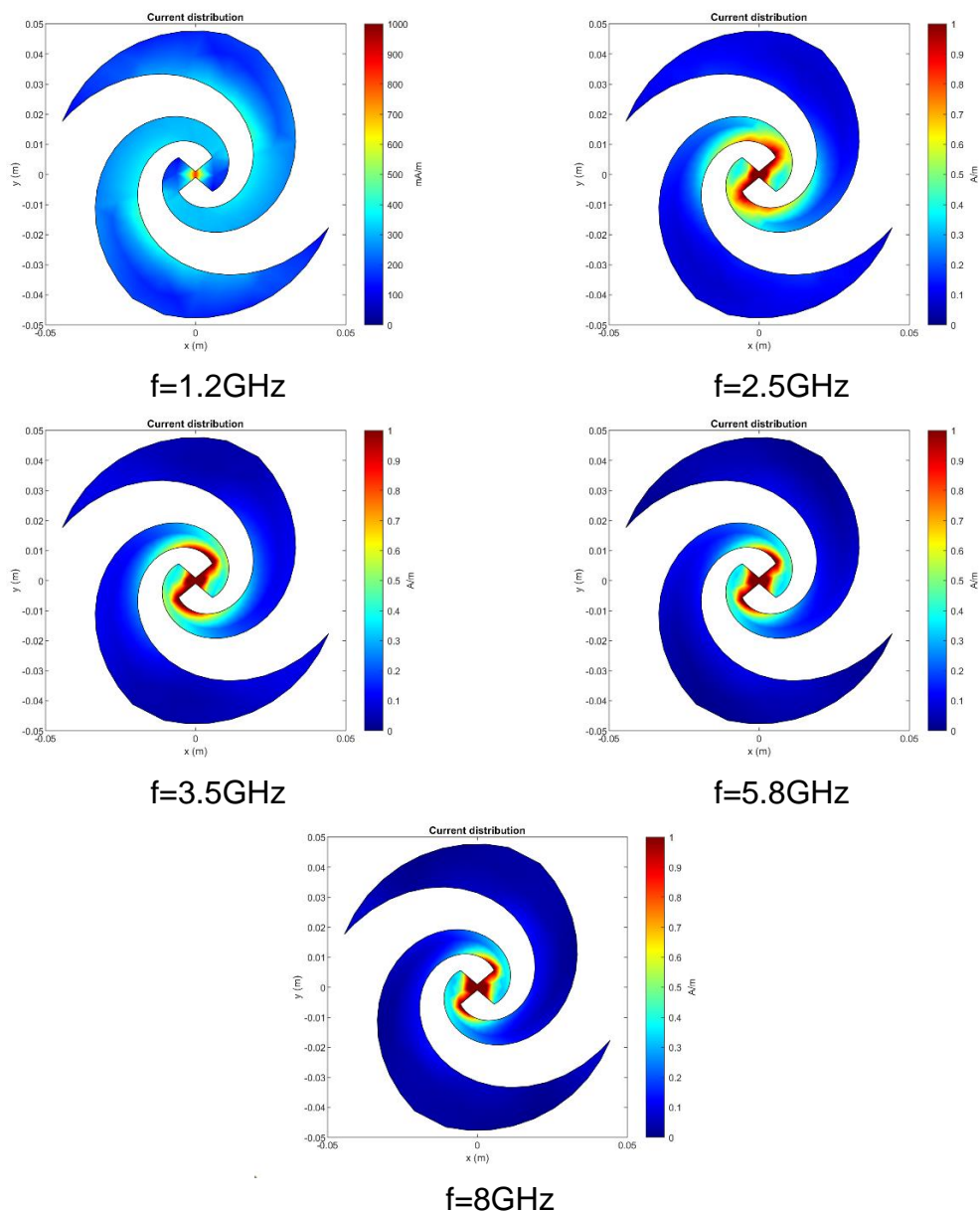

f=1.2GHz

f=2.5GHz

f=3.5GHz

f=5.8GHz

f=8GHz

Figure 38: Current distributions for different frequencies for the first simulated antenna

28

From *Figure 38*, it results evident that for the lower frequency, the currents are more evenly distributed in the arms. For the center of the operating band and the higher one, the currents concentrate around the feed. The behavior is the expected according to section 2.1: The currents decay rapidly from the center of the antenna for self-scaling structures. Since the best antenna performance has been obtained at the design center frequency, it is concluded that optimum antenna performance requires that the currents be concentrated around the feed and do not travel along the source arms. This will be further analyzed when a reflector plane is added to back the antenna in next subsections.

2.7. Comparison with other spiral antennas

To justify the selection of equiangular spiral antennas, it is necessary to compare their performance with that of other types of antennas, so that the advantages they offer can be determined. Since the design parameters of rectangular spiral antennas differ from those of equiangular spiral antennas, it is necessary to choose a reference that allows a real comparison. For this purpose, an antenna with a conductor width of 10 mm, like that obtained in the first simulated antenna, and a conductor length of about 300 mm has been chosen to approximate the physical dimensions of the first antenna. The code for generating the new rectangular *spiralAnt* object is as follows:

```
%Generation of rectangular spiral antenna
spiralAnt = spiralRectangular('NumArms',2,'InitialLength',0.02,...,
'InitialWidth',20e-3,'Spacing',10e-3,'StripWidth',10e-3);
nT = rectspirallength2turns(spiralAnt,300e-3);
spiralAnt.NumTurns=nT;
```

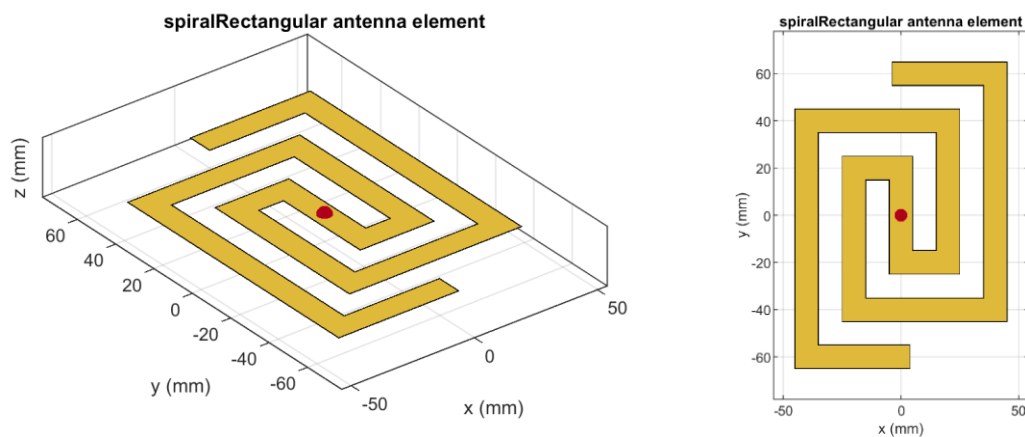*Figure 39: Code for the generation of rectangular spiral antenna*

Figure 40: Generated two-arms rectangular spiral antenna

The *spiralRectangular* command creates a rectangular spiral antenna object, to which the initial length, the initial width, the spacing between the conductors and the width of the conductor are specified. The number of turns is calculated with the command *rectspirallength2turns*, passing as parameter the desired total length of the conductor. Once the object from *Figure 40* was created, the same simulations were performed as in section 2.6, using the same code used between sections 2.6.1 and 2.6.6 without any changes. The results of the comparison and the justification for using the equiangular spiral antenna are:
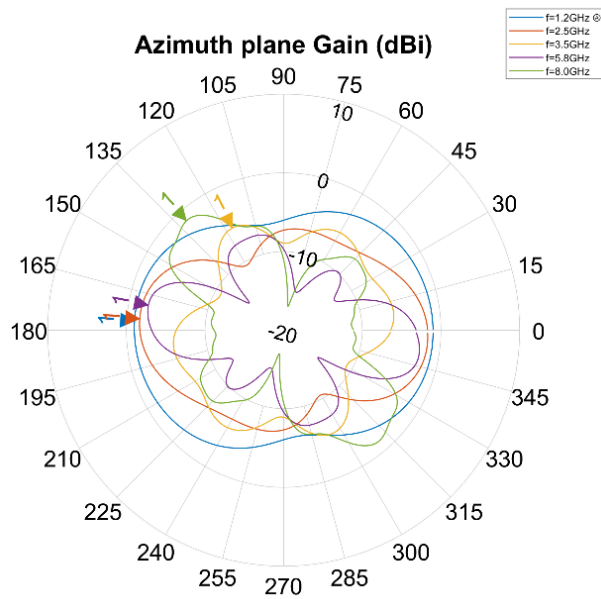
2.7.1. 2D Radiation diagrams

Figure 41: Azimuth plane gain for the first simulated antenna

Frequency	Degrees (⁰)	Magnitude (dBi)
1.2GHz	176.5	-1
2.5GHz	175.5	-1.6
3.5GHz	116.7	-5.5
5.8GHz	169.5	-2.5
8GHz	131.6	-1.4

Table 3: Azimuth plane gain maximums

As with the equiangular antenna, the rectangular antenna has extremely low gain in the azimuth plane (*Figure 41*), which is the plane in which the antenna physically rests. This is expected since the radiation should be perpendicular to the antenna itself.
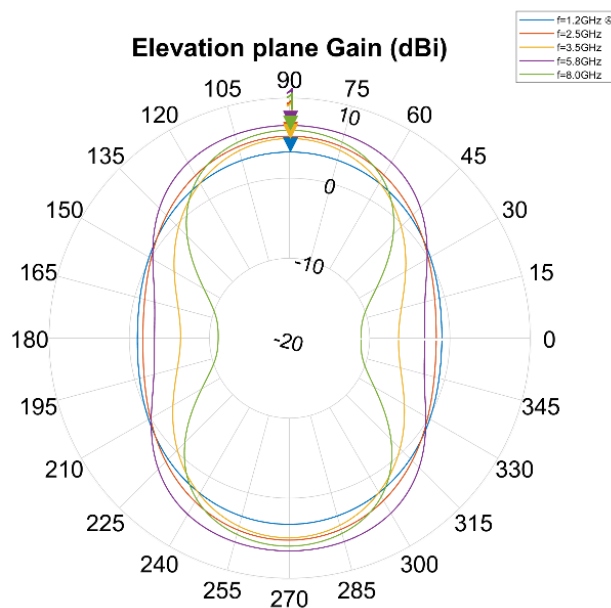

Figure 42: Elevation plane gain for the first simulated antenna

30

Frequency	Degrees (⁰)	Magnitude (dBi)
1.2GHz	89.8	3.3
2.5GHz	89.8	5.3
3.5GHz	89.8	5
5.8GHz	89.8	6.6
8GHz	89.8	6

Table 4: Elevation plane gain maximums

In this section we find maximum gain values comparable and even slightly higher than those of the equiangular antenna evaluated in section 2.6.1. However, it can be observed that the gain does not follow an apparently predictable pattern like that of the equiangular antenna but varies continuously at each frequency evaluated. This represents a disadvantage compared to such an antenna.
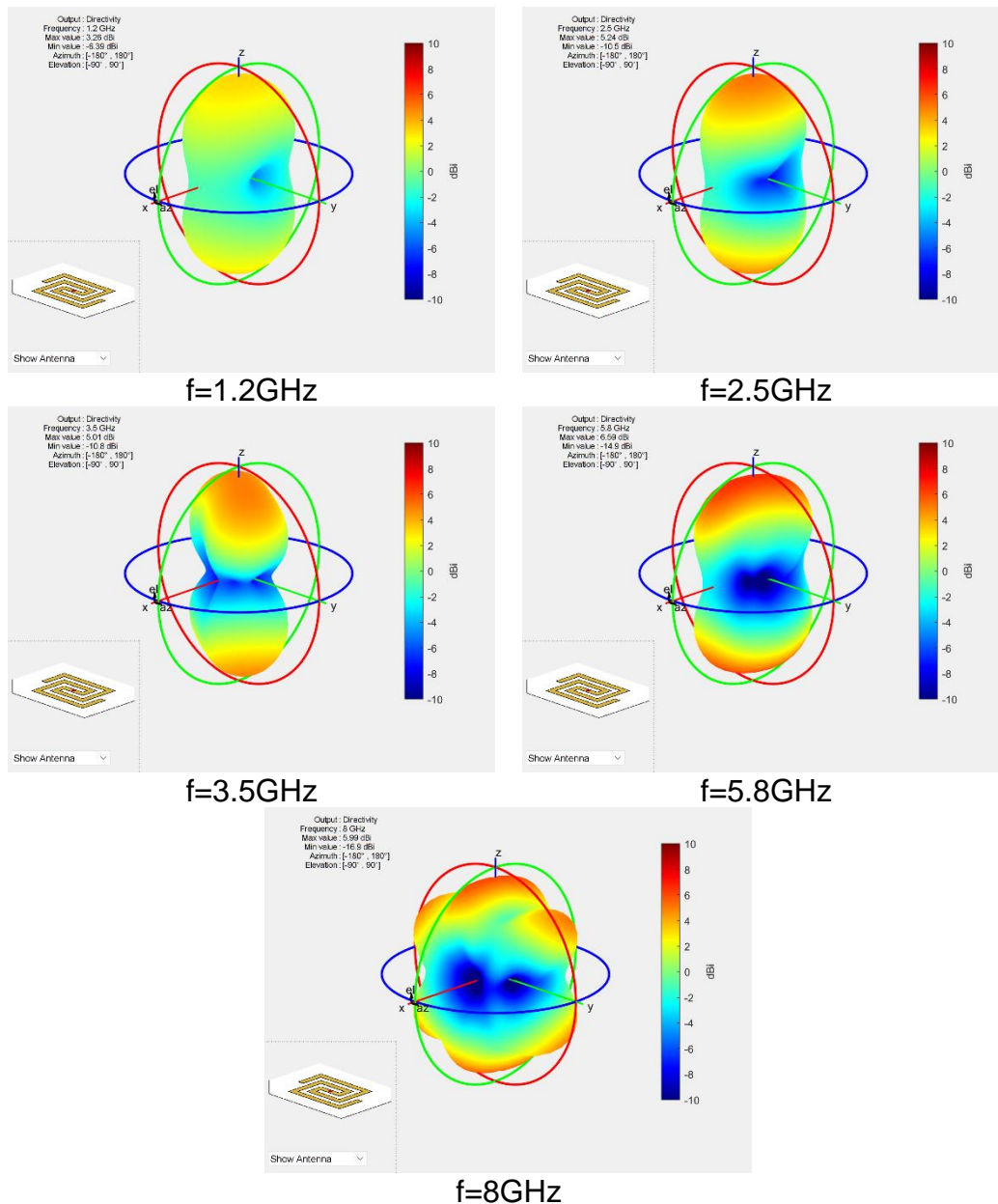
2.7.2. 3D Radiation diagrams

f=1.2GHz

f=2.5GHz

f=3.5GHz

f=5.8GHz

f=8GHz

Figure 43: 3D radiation diagrams for different frequencies for the first simulated antenna

31

Figure 43 shows that the rectangular antenna has constant radiation patterns within the 1GHz-6GHz band. However, it is clearly observed that the pattern begins to suffer deformations at high frequencies, which did not occur with the equiangular antenna, even outside its design operating range.
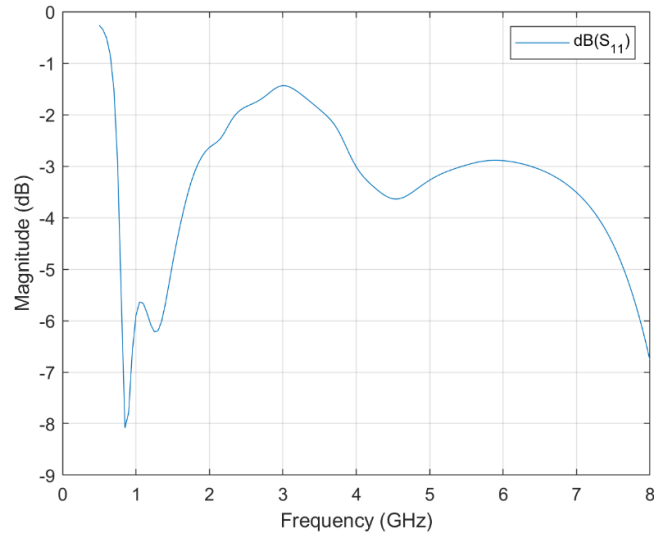
2.7.3. S_{11} parameter

Figure 44: S_{11} parameter versus frequency for first simulated antenna

In terms of impedance matching, *Figure 44* shows that the rectangular antenna is at a clear disadvantage compared to the equiangular antenna (*Figure 31*). The antenna is only found with an S_{11} parameter of less than -5dB between approximately 0.9GHz and 1.5GHz and again around 8GHz, a much smaller frequency range than the equiangular antenna can operate in, as well as being discontinuous and difficult to match.

2.7.4. Input impedance
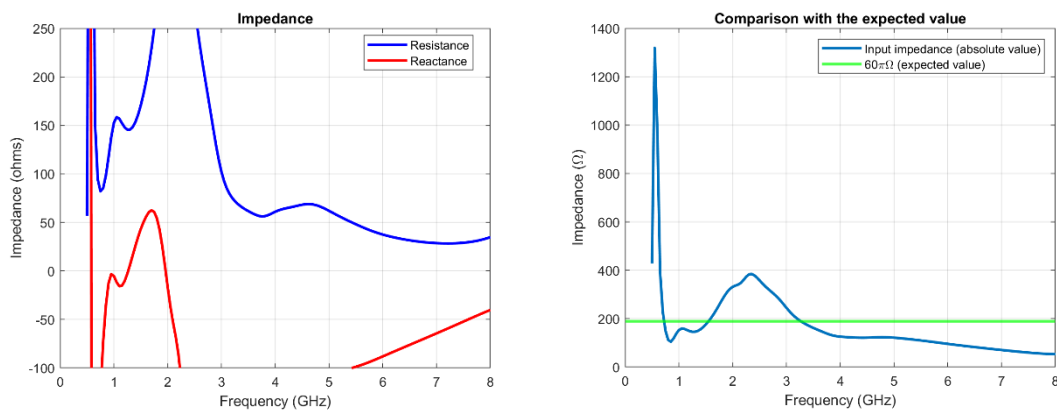
Figure 45: Input impedance versus frequency for first simulated antenna

The input impedance plots of *Figure 45* match that seen with parameter S_{11}. Both resistance and reactance are highly unstable throughout the range analyzed. The absolute value of the impedance varies between 160Ω and 400Ω between 1GHz and 3GHz, steadily decreasing after this frequency. The input impedance deviates from the nominal $188\ \Omega$ because it is not a self-complementary structure.

2.7.5. Axial ratio
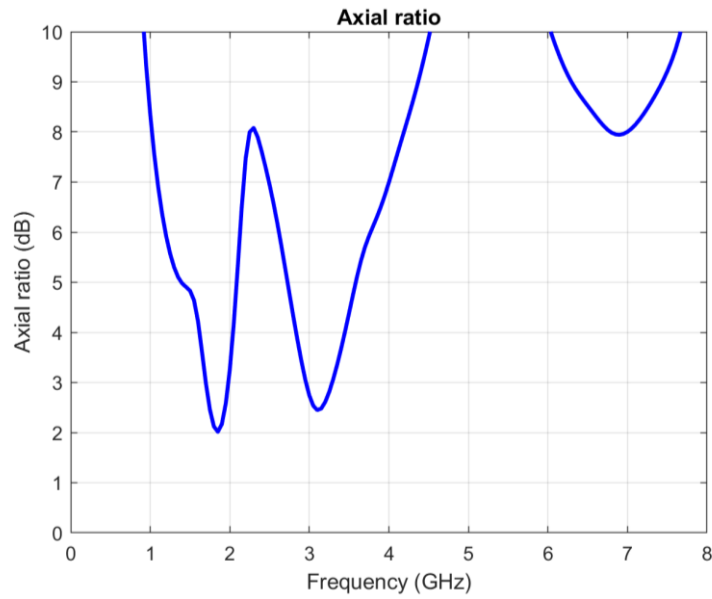
Figure 46: Axial ratio versus frequency for first simulated antenna

The axial ratio of the rectangular antenna remains high, barely reaching the value of 2dB for a frequency slightly less than 2GHz, as can be seen in *Figure 46*. Therefore, it can be said that the antenna has an elliptical polarization for most of the studied frequencies and is not applicable for use cases that require circular polarization.

2.7.6. Surface currents distributions

f=1.2GHz

f=2.5GHz

f=3.5GHz

f=5.8GHz

33
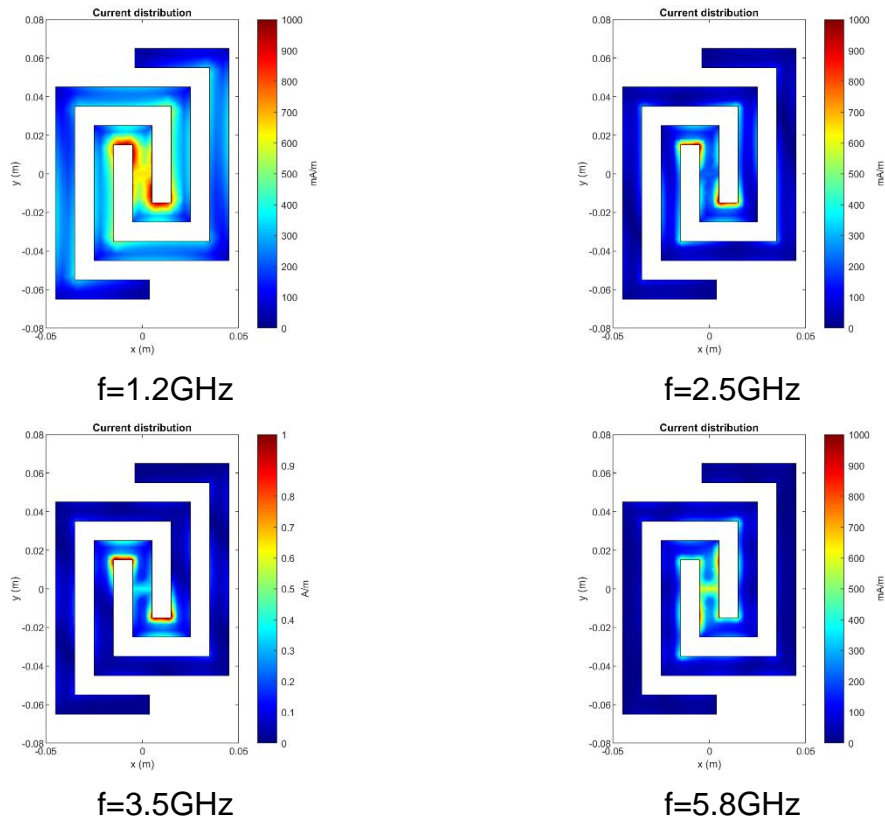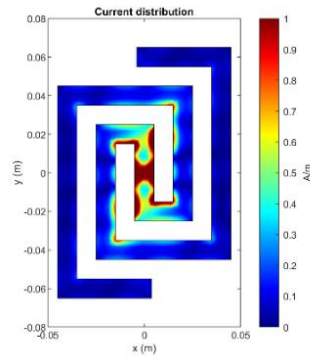
f=8GHz

Figure 47: Current distributions for different frequencies for the first simulated antenna

As was the case with the equiangular antenna, it can be seen from *Figure 47* that the currents are distributed more dispersedly at low frequencies. However, the stable behavior observed in section 2.6.6 for the higher frequencies is no longer present, as the results obtained display a rather erratic distribution of the currents, which go from concentrating around the first turn of the arms to be around the source and beginning to be distributed with to the arms as the operating frequency increases. This is a direct result of this type of antenna not being a self-scaling structure as discussed in section 2.1.1.

In general, it has been observed that a rectangular spiral antenna of similar physical dimensions does not present any advantage over the equiangular antennas studied so far that justify its use. Undoubtedly, both frequency-independent behavior in most parameters and circular polarization have been lost. Therefore, the choice of equiangular spirals is justified in this way, and they were continued to be used in the next simulations.

2.8.   Influence of the growth rate

As mentioned in section 2.6, the other physical parameter that can be modified is the growth rate (and with it, the number of turns the spiral makes). To determine the influence of this parameter, simulations will be conducted and analyzed by varying the growth rate values presented in the previous section (for approximately 0.5, 1 and 2 turns).

```
%Set the growth rate for N approx. 0.5, 1 and 2
spiralAnt.GrowthRate=0.57;
spiralAnt.GrowthRate=0.28;
spiralAnt.GrowthRate=0.14;
```

Figure 48: Code to generation of rectangular spiral antenna

With these values set, the same parameters from the previous section can be simulated in a simple way. Most of the previous simulations were conducted for each rate and the results were stored in variables for representing them together later. The 3D diagrams and currents distributions were omitted since it would require an excessive number of commands to perform. The code is not included in this document for reasons of space but is included as an appendix (6.2). The results are shown and discussed below.

34

2.8.1. Azimuth plane radiation diagram

f=1.2GHz
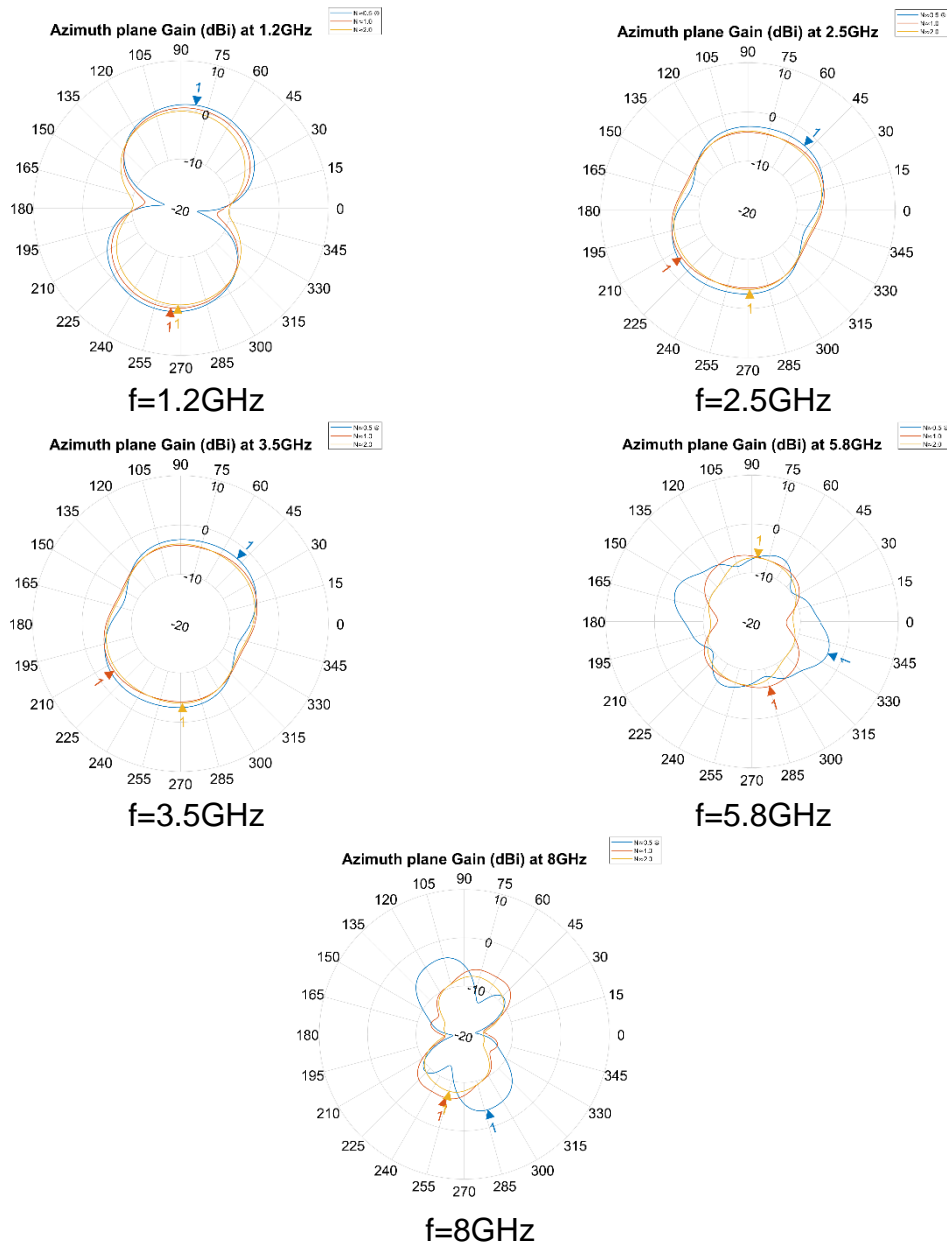
f=2.5GHz

f=3.5GHz

f=5.8GHz

f=8GHz

Figure 49: Comparison of the azimuth plane patterns for different frequencies and turns

For the azimuth plane, *Figure 49* shows that the biggest variations appear when the number of turns is low (in this specific case, under one complete turn), especially in the middle-to-higher frequencies studied. For the number of turns tht surpass the unity, the values remained consistent. The values of the gain remain extremely low as expected, below the 0dBi mark in all cases.

This is the expected behavior as exceedingly little electromagnetic radiation is supposed to occur in the direction parallel to the plane that contains the antenna, and it is consistent even changing the number of turns the antenna makes. The variations that appear are extremely small to even be considerable for electromagnetic radio communications.

2.8.2. Elevation plane radiation diagram

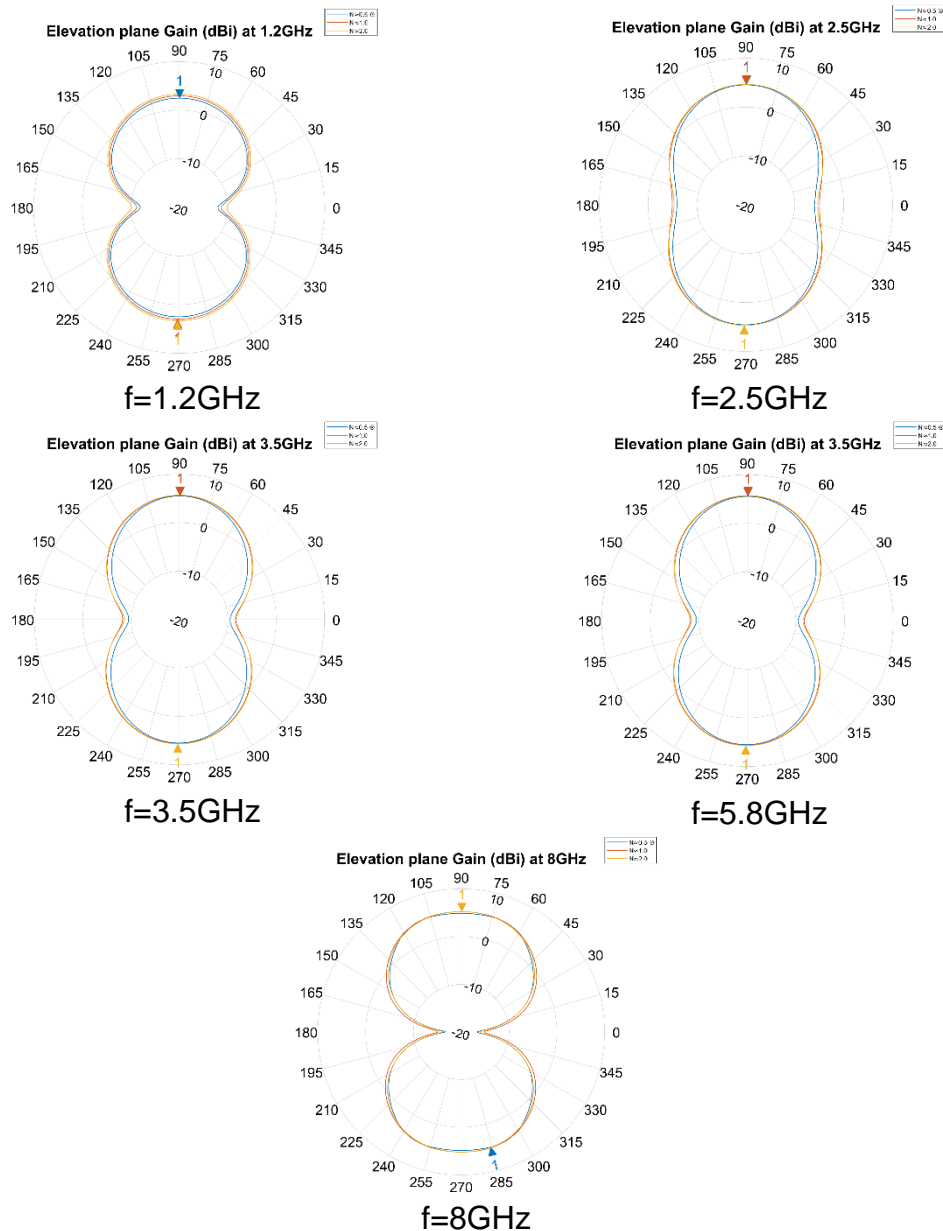f=1.2GHz

f=2.5GHz

f=3.5GHz

f=5.8GHz

f=8GHz

Figure 50: Comparison of the elevation plane patterns for different frequencies and turns

For the elevation plane, it can be seen from *Figure 50* that the results are consistent regardless of the number of turns the antenna has. The gain is slightly better for the antenna with the higher number of turns, but with exceedingly small variations. The gains obtained were around 2.5dBi for the 1.2GHz frequency measurement and slightly over 5dBi for the rest of measurements.

Again, the behavior is the expected as the biggest part of the electromagnetic radiation occurs in the direction perpendicular to the antenna plane. The graphs show extraordinarily little variations as the number of turns the arms of the antenna make, remaining consistent in the three scenarios evaluated. This, together with the previous results, allows us to conclude that the gain is not significantly affected by the number of turns made by the antenna.
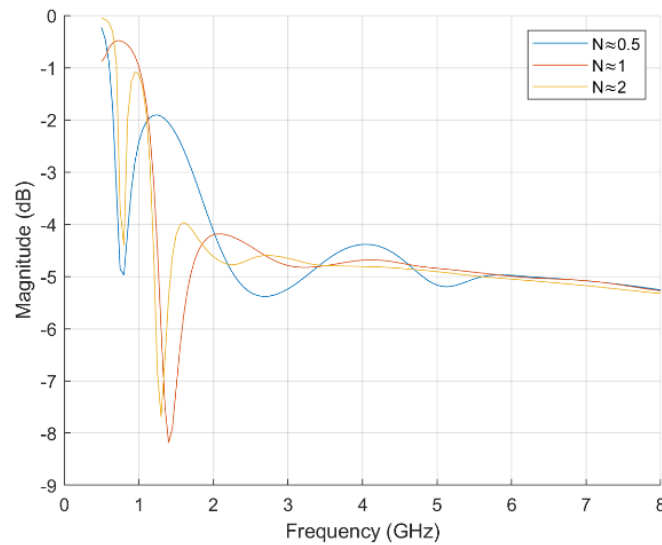
2.8.3. S₁₁ parameter

Figure 51: Comparison of the S₁₁ parameter for different number of turns

The reflection coefficient displayed in *Figure 51* seems to improve with the number of turns added. The curve becomes more stable, and its value approaches the starting frequency of 1GHz more quickly. The smaller number of turns used (0.5) creates evident oscillations in the lower frequencies, which is highly undesirable in the antenna design field.
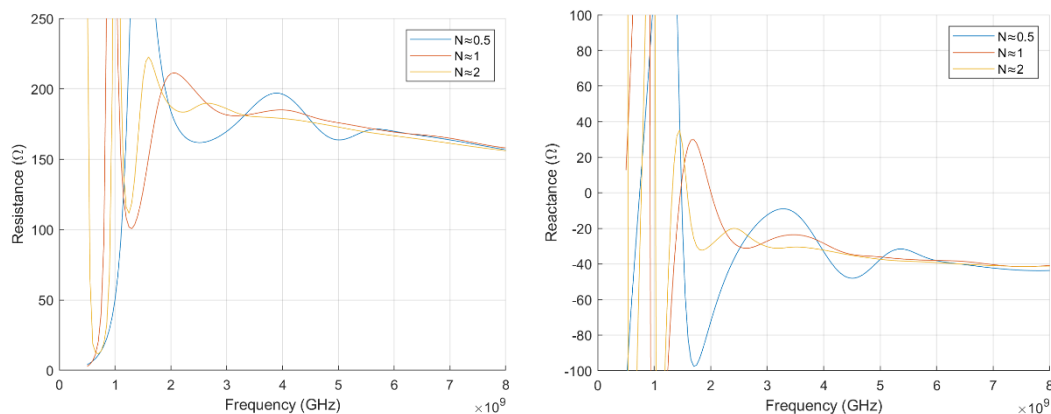
2.8.4. Input impedance

Figure 52: Comparison of the input impedance for different number of turns

As it can be seen in *Figure 52*, the input impedance remains stable for the operating band, but again performs best with the highest number of turns (in general). The resistance reaches a point of about 180Ω and slowly goes down from there. The antenna exhibits capacitive behavior as expected, since the spiral arms are greatly coupled and will inherently cause parasitic capacitors to appear. This is especially seen for the largest number of turns, which have strong capacitive behavior around the low operating frequency of 1GHz, because this frequency is defined from the minimum operating radius, where the arms are closest to each other.
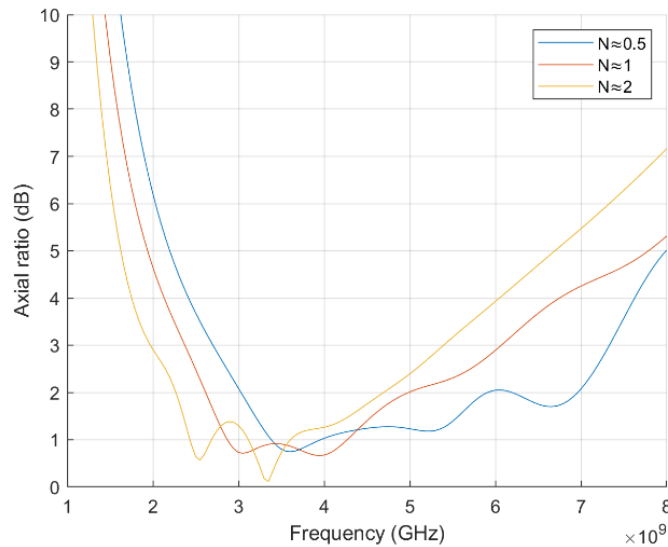
37

2.8.5. Axial ratio

Figure 53: Comparison of the axial ratio for different number of turns

Again, the results are consistent regardless of the number of turns the antenna has, but with a catch: *Figure 53* shows that the axial ratio gets better for the lower operating frequencies when increasing the number of turns but displayed better results for the higher operating frequencies when the antenna had only 0.5 turns.

2.8.6. Optimization

Since the growth rate and the number of turns seem to exhibit a strong influence in the performance of the antenna, it is interesting to analyze which value would produce a better-performing antenna. MATLAB includes an optimizer tool within the Antenna Toolbox. After setting the desired properties of the antenna object, it allows you to select other properties to optimize based on the maximum gain or other parameters. In this case, the desired property to optimize is the growth rate. A series of one hundred iterations was performed between a value of 0.1 and 1 and after a few moments it is obtained that the best value of this rate as a function of maximum gain is 0.16 (that is, slightly above 1.78 turns). The optimized antenna can be seen in *Figure 54*.
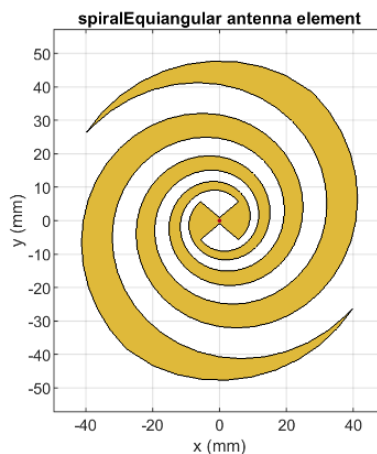

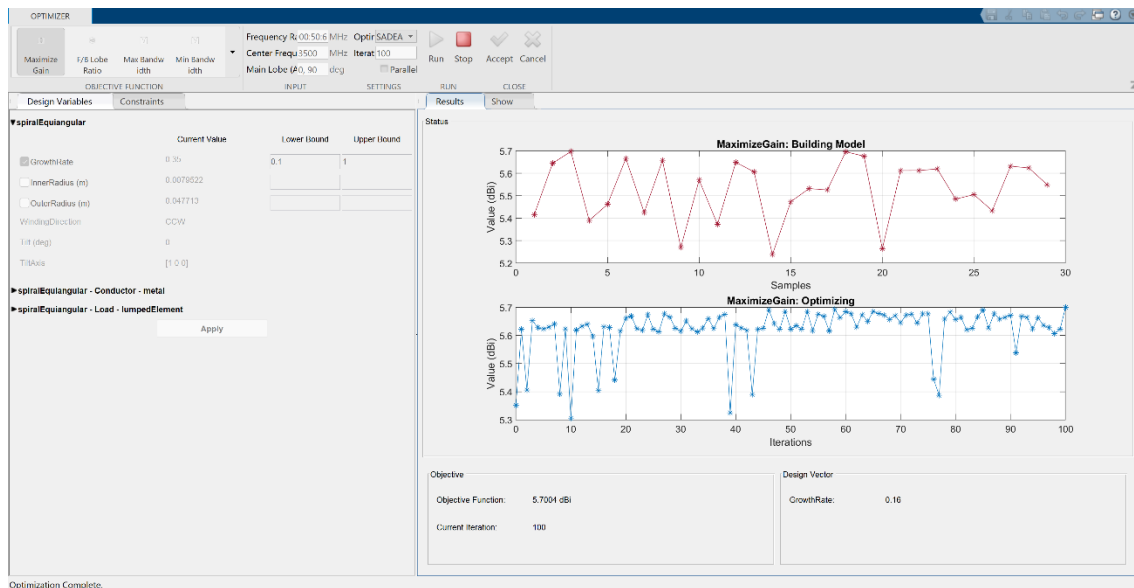*Figure 54: Generated gain-optimized antenna*

38

Figure 55: MATLAB antenna parameter optimizer interface

A simple manual for using the MATLAB antenna optimizer tool (*Figure 55*) has been created as an appendix and can be found in section 6.2. In this manual, the optimization process for parameters other than gain, such as F/B ratio, bandwidth, and antenna size minimization is explained.

2.9. Reflector-backed antenna

The next step will be creating an infinite reflector plane to back the antenna and analyze its effects on the parameters of the antenna. The most obvious implication of adding a reflector plane is that the radiation will no longer be bi-directional. The back lobe will be removed. Also, the maximum gain should improve as a direct consequence of such removal. The simulations are to be done with an infinite plane of a perfect conductor (PEC) and with an initial spacing of $\lambda/4$ (considering the center frequency 3.5GHz).

```
%Create a reflector plane excited by the previously defined antenna
rf = reflector;
rf.GroundPlaneLength = inf;
rf.GroundPlaneWidth = inf;
rf.Exciter = spiralAnt;
rf.Spacing = 0.0214;
```

Figure 56: Code to create a reflector plane excited by the previously defined antenna

In this case, a new reflector plane object arbitrarily named rf is created. An infinite size is specified in its dimensions. The exciting antenna and its separation from the plane are also selected, as seen in *Figure 57*. The code needs the antenna object *spiralAnt* to be created beforehand. The parameters used for the equiangular antenna are the same one from the previous simulations and the growth rate is set to the optimized value of 0.16. All the parameters can be simulated using the same commands from the first section, changing the object from the antenna (*spiralAnt*) to the reflector plane object (*rf*). The results are presented and discussed in the next subsections.

39
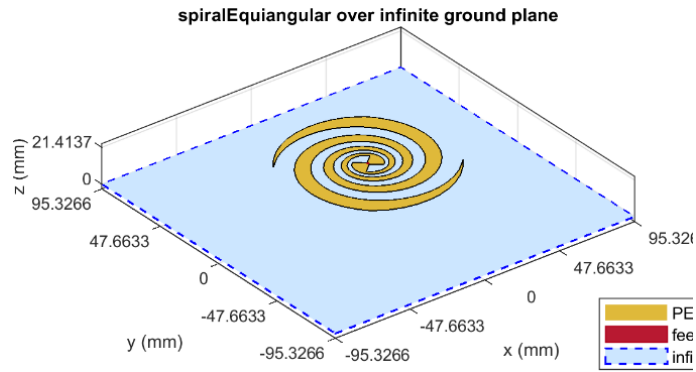
Figure 57: Generated equiangular antenna over an infinite ground plane

2.9.1. 2D Radiation diagrams
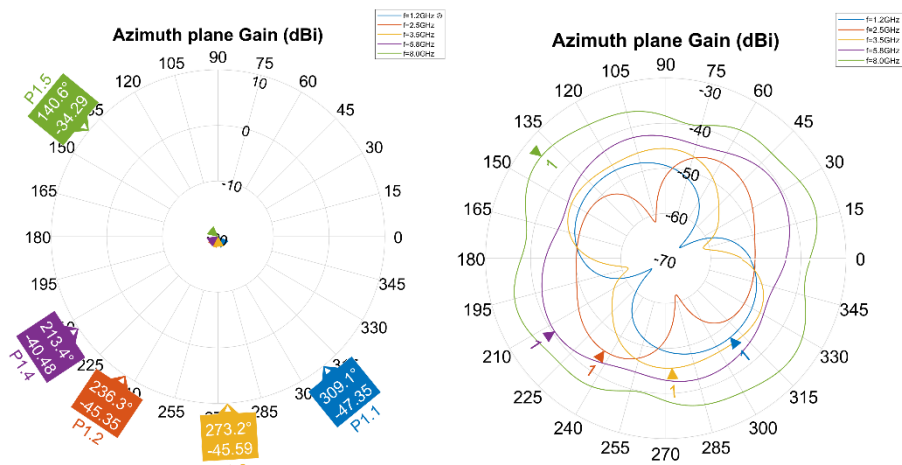
Figure 58: Azimuth plane gains for the reflector-backed antenna

In the azimuthal plane, we obtain extremely low gain values, below the -40dBi mark (*Figure 58*). This means that the reflector further decreases the radiation to the sides of the antenna, making it almost null. This is the expected behavior for reflectors, as they concentrate the energy in the direction perpendicular to the plane.

Figure 59: Elevation plane gains for the reflector-backed antenna

40

The diagram in the elevation plane seen in *Figure 59* shows how the power is concentrated very symmetrically in the opposite direction to the reflector plane. The gain is increased by about 3dB on average with respect to the antenna without any reflector. Th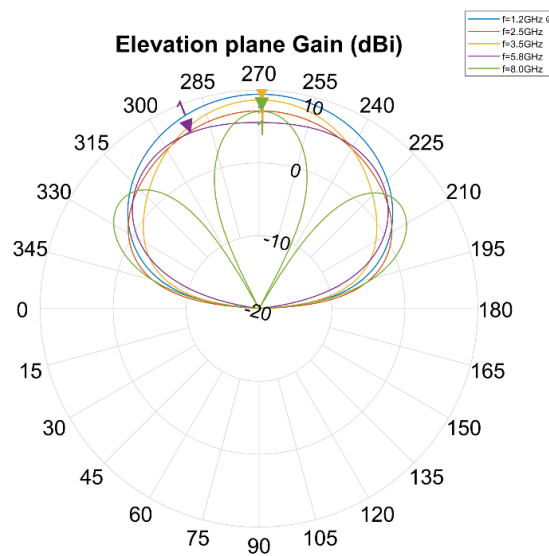is improvement in the radiation pattern is especially evident at the lower frequencies, where even the best relative gain of the three is obtained, in contrast to the case without reflector, where the gain was affected at these frequencies. In the frequency that was outside of the operating range (8GHz), nulls start to appear, degrading its quality.

2.9.2. 3D Radiation diagrams

f=1.2GHz

f=2.5GHz

f=3.5GHz

f=5.8GHz

f=8GHz
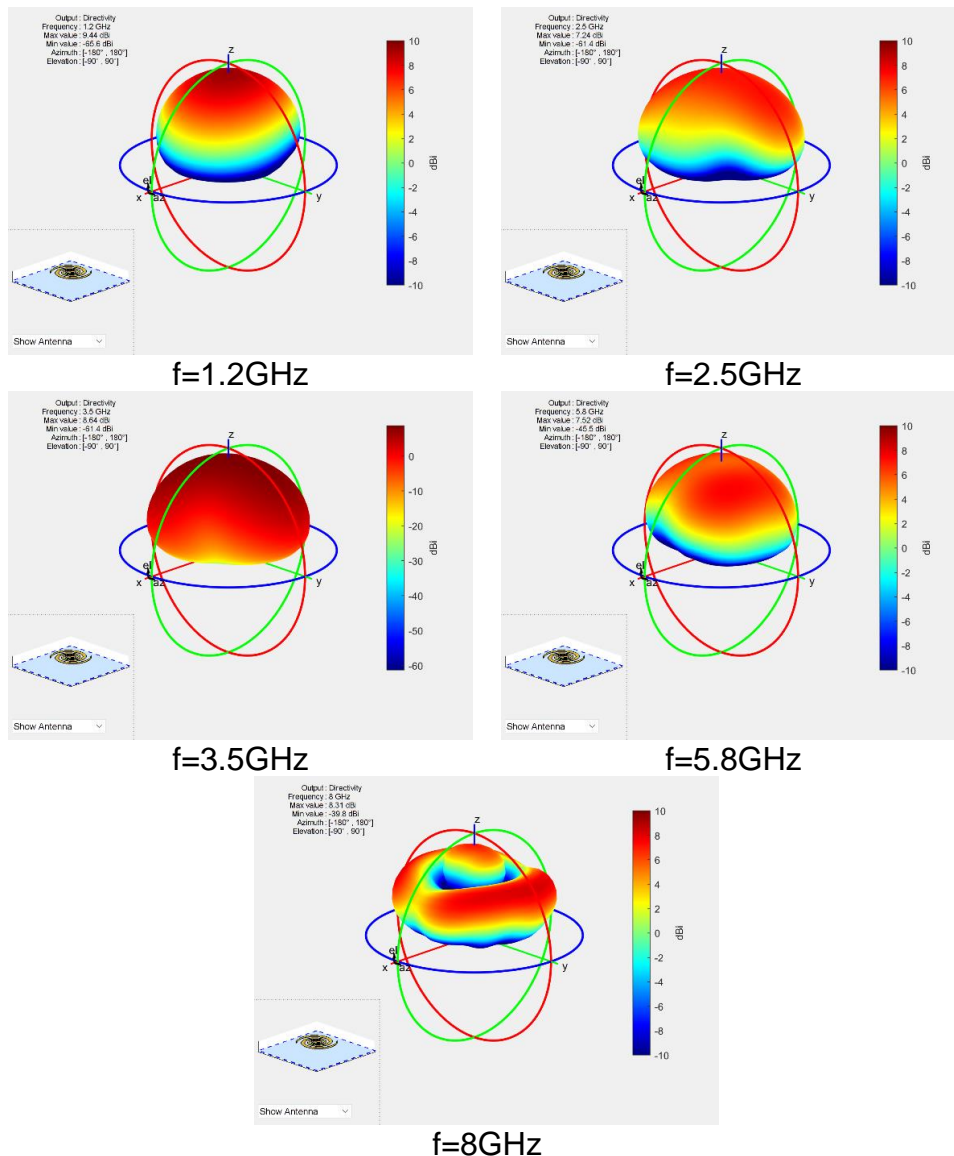
Figure 60: 3D radiation diagrams of the reflector-backed antenna

The three-dimensional radiation pattern seen in *Figure 60* shows good symmetry at the study frequencies. The unidirectional radiation gate produced by the addition of the reflector plane is clearly observed and well maintained over the large frequency range of 5GHz in study. At the higher frequency, outside of the design frequency, the pattern starts to display the appearance of lobes, so that its efficiency in certain directions is degraded.

2.9.3. S_{11} parameter

Figure 61: S_{11} parameter for the reflector-backed antenna

The reflection coefficient seen in *Figure 61* displays important oscillations below 3GHz, varying approximately between -2.5dB and -7.5dB. Apart from this oscillation, the matching has similar values to those of the single antenna from around 3GHz up, concentrating the parameter around -5dB.
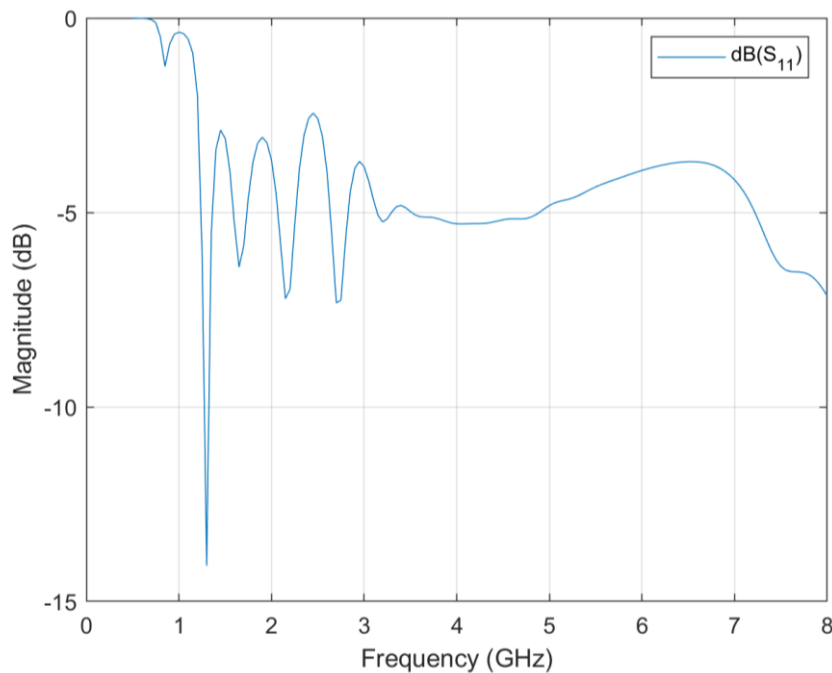
2.9.4. Input impedance
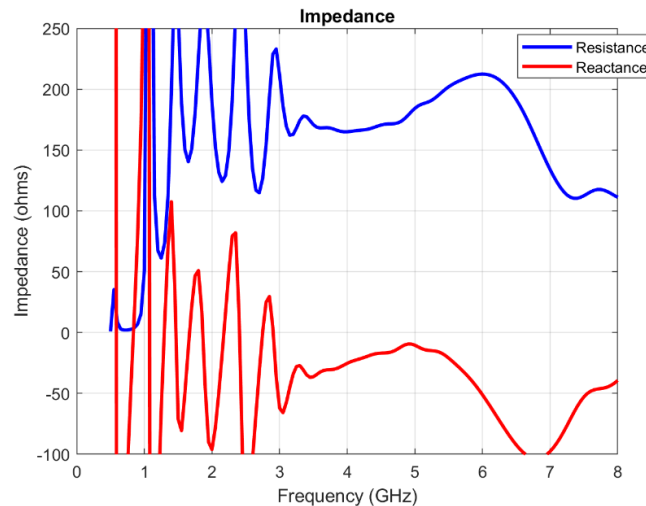
Figure 62: Input impedance for the reflector-backed antenna

As could be observed with parameter S_{11}, the impedance shown in *Figure 62* presents oscillations at frequencies below 3GHz, varying in its real part between 125Ω and 250Ω and its imaginary part reaching even positive values (changing to an inductive behavior). It results apparent then that the reflector plane increases the capacitive behavior of the system due to the inherent capacitance created between the antenna and the reflector.

2.9.5. Axial ratio
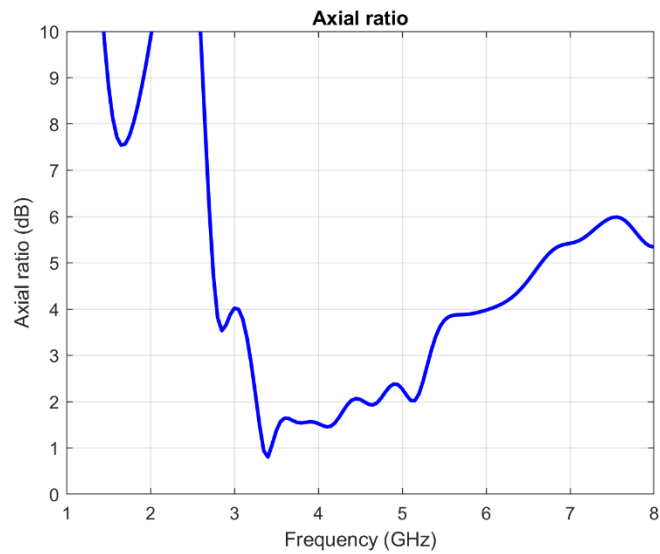
Figure 63: Axial ratio of the reflector-backed antenna

As it can be seen in *Figure 63*, the axial ratio presents an excellent performance again at frequencies higher than 3GHz, especially between 3.2GHz and 5.2GHz, where this rate is quite flat and lower than 3dB. In the range between 1 and 3GHz values higher than 5dB are evidenced, which represents an elliptical polarization that can become undesirable.

2.9.6. Surface currents distribution

f=1.2GHz

f=2.5GHz

f=3.5GHz

f=5.8GHz

43
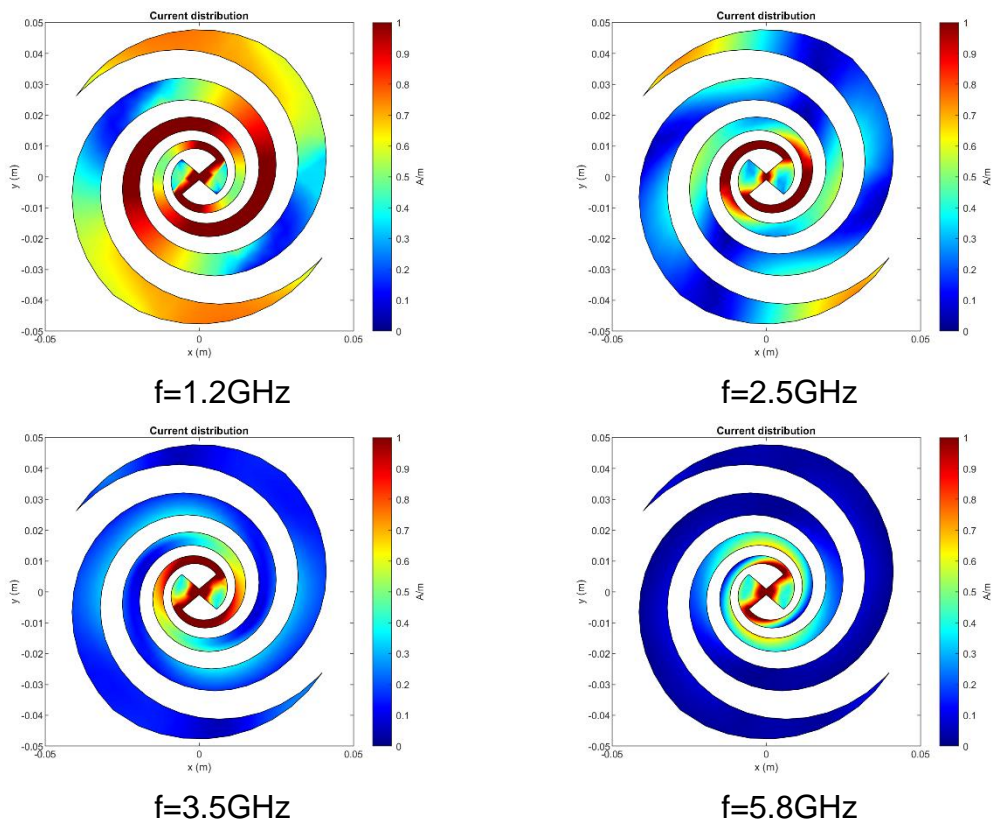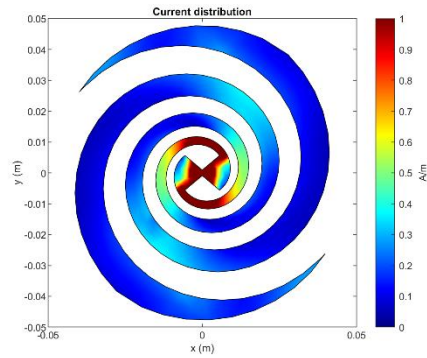
f=8GHz

Figure 64: Current distributions for different frequencies for the reflector-backed antenna

As in the case without reflector, *Figure 64* shows that the currents are concentrated around the source as the antenna performance improves. For the design center frequency, it is evident that the currents are at the beginning of the arms and do not extend to the tips of the arms. For the lower frequencies, the currents are more distributed around the arms, which evidences a non-self-scalable behavior, clearly seen in the impedance plot, where oscillations can be seen in such frequencies.

3. Conclusions and future work

The work makes an in-depth description of equiangular spiral antennas. The main conclusion obtained is that this type of antenna fulfills to a good extent each of the theoretical approaches raised in section 2.1: frequency independence, good circular polarization, and small size. The principle of operation of self-scaling and self-complementary structures has been fully demonstrated: antennas can be defined by angles and within a wide frequency range can be observed as a scaled version of themselves, clearly observed in the surface current plots.

Compared to other spiral structures, such as the well-studied rectangular spiral antenna, equiangular spiral antennas have clear advantages in all parameters. Although rectangular antennas presented similar gain values to equiangular antennas, they could only operate with impedance matching in a very narrow frequency band. The polarization of an antenna of considerable dimensions was highly elliptical in the whole frequency band studied, unlike the equiangular antenna that presented good circular polarization in a range of more than 3GHz.

The MATLAB suite with its Antenna Toolbox has proved to be suitable for carrying out each of the simulations required for different types of antennas, such as: radiation patterns in two and three dimensions, S_{11} parameter, input impedance, axial ratio, and surface current distribution. Additionally, the same application also serves as a parametric optimization tool, another point in favor of its use.

Another conclusion obtained is that the use of a reflector plane can effectively convert the radiation pattern into a unidirectional one, sacrificing stability in the input impedance at low frequencies, resulting in a lower effective bandwidth than expected without the presence of the reflector, which in turn affects the maxim of this type of antennas: frequency independence.

At the end of this work, it is determined that the objectives have been fully achieved: different spiral antennas, such as the equiangular and rectangular, have been analyzed and their characteristics and design parameters have been studied. With this, different configurations of the equiangular antennas have been simulated and the effect of the variation of the number of turns on their behavior has been observed. Finally, it has been determined that the tool is useful to perform this type of simulations, not only of simple equiangular spiral antennas, but with the possibility of adding parasitic elements such as reflector planes.

The original planning has been fully respected, and the progress made has been discussed with the tutor in periodic meetings that were linked to the achievement of the objectives set. The proposed methodology is considered adequate as each of the proposed objectives was achieved, so that it has not been necessary to make considerable modifications to the work during its execution phase.

The sustainability impacts discussed at the beginning of the paper can be observed if this type of antennas is implemented for more applications in the future. Also, as future work, simulations can be explored that include improvements proposed by other authors, such as additional parasitic elements, cavity structures filled with insulating material, toothed spirals, among others.

4. Glossary

- PEC: Perfect electrical conductor.
- R_{max}: Outer radius of the spiral.
- R_{min}: Inner radius of the spiral
- f_{hi}: Highest operating frequency.
- f_{low}: Lowest operating frequency.
- TEM: Transversal electromagnetic.
- S_{11}: input port voltage reflection coefficient.

5. Bibliography

Anguera, J., & Pérez, A. (2008). *Teoría de Antenas.* Universitat Ramon Llull.

Aznar, Á., Roca, L., Casals, J., Robert, J., & Boris, S. (2002). *Antenas.* Edicions de la UPC, S.L. Retrieved from https://books.google.es/books?id=AlQ8p2C4sCoC

Balanis, C. (2015). *Antenna Theory: Analysis and Design.* Wiley. Retrieved from https://books.google.es/books?id=PTFcCwAAQBAJ

Fu, W., Lopez, E. R., Rowe, W. S., & Rowe, W. S. (2010, May 5). A Planar Dual-Arm Equiangular Spiral Antenna. *IEEE Transactions on Antennas and Propagation*, pp. 1775 - 1779.

García Martínez, S., Sánchez Olivares, P., Fernández González, J. M., & Tamayo Domínguez, A. (2022). Equiangular Spiral Antenna Design Embedded in a Launcher Fuselage for S-Band Communications. *2022 16th European Conference on Antennas and Propagation (EuCAP)* (pp. 1-5). Madrid, Spain: IEEE.

Garufo, A., Llombart, N., & Neto, A. (2016, October 10). Radiation of Logarithmic Spiral Antennas in the Presence of Dense Dielectric Lenses. *IEEE Transactions on Antennas and Propagation*, pp. 4168 - 4177.

Jeon, J. H., Chang, J. T., & Pham, A.-V. (2014). Band-notched UWB equiangular spiral antenna. *2014 IEEE Antennas and Propagation Society International Symposium (APSURSI)* (pp. 1323-1324). Memphis, TN, USA: IEEE.

Nakano, H., Kikkawa, K., Iitsuka, Y., & Yamauchi, J. (2008, August 8). Equiangular Spiral Antenna Backed by a Shallow Cavity with Absorbing Strips. *IEEE Transactions on Antennas and Propagation*, pp. 2742-2747.

Rumsey, V. H. (1957). Frequency independent antennas., *5*, pp. 114-118.

Sakomura, E. S., Ferreira, D. B., Bianchi, I., & Nascimento, D. C. (2018). Compact Planar Two-Arm Compound Spiral Antenna for L-/X-Band Direction Finding Applications. *2018 IEEE International Symposium on Antennas and Propagation & USNC/URSI National Radio Science Meeting* (pp. 853-854). Boston, MA, USA: IEEE.

Sirbu, B., Tekin, T., & Pouhè, D. (2014). Design and simulation of an equiangular spiral antenna for extremely high-frequencies. *The 8th European Conference on Antennas and Propagation (EuCAP 2014)* (pp. 3102-3106). The Hague, Netherlands: IEEE.

Sugak, M. I., Ballandovich, S. V., Kostikov, G. A., Antonov, Y. G., & Liubina, L. M. (2018). Modernized logarithmic spiral antenna with reduced sizes. *2018 IEEE Conference of Russian Young Researchers in Electrical and Electronic Engineering (EIConRus)* (pp. 521-523). Moscow and St. Petersburg, Russia: IEEE.

Tavakoli, A., Fard, A., & Moini, R. (1996). Analysis of dual-arm logarithmic spiral microstrip patch antennas. *IEEE Antennas and Propagation Society International Symposium. 1996 Digest* (pp. 1078-1081). Baltimore, MD, USA: IEEE.

Veysi, M., & Kamyab, M. (2011, November 11). Bandwidth Enhancement of Low-Profile PEC-Backed Equiangular Spiral Antennas Incorporating Metallic Posts. *IEEE Transactions on Antennas and Propagation*, pp. 4315 - 4318.

6. Appendices

6.1.   MATLAB Antenna Toolbox and optimizer manual

MATLAB, starting with version 2020b, incorporates a graphical tool for antenna design. Apart from including a diverse catalog of antennas that can be easily simulated, it also incorporates a parametric antenna optimization tool, which will be especially useful in the design and creation of antenna elements. To use the application, it is necessary to have it installed, as it is not part of the MATLAB code base. However, it is included by default in the installer of all editions from the one mentioned above. To open the application, select the "APPS" tab at the top of MATLAB and pull down the menu. The application can be found in the "Signal Processing and Communications" section, as shown in *Figure 65*.
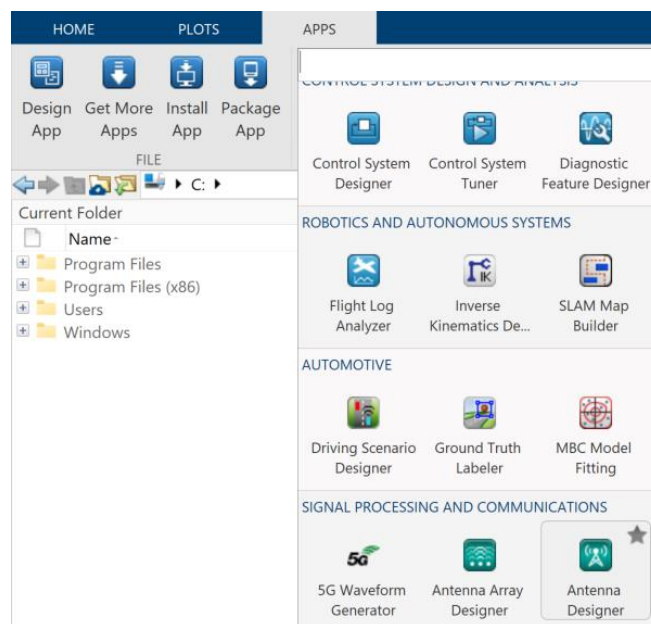

Figure 65: Antenna Designer application selection

Once the application is open, select the "New" button in the top menu, as it can be seen in *Figure 66*. This will create a blank antenna object that will serve as the basis for subsequent designs and simulations.
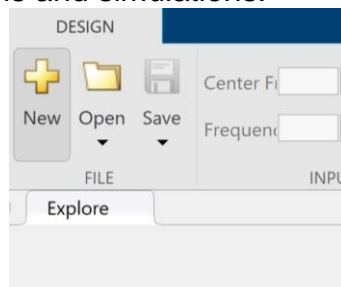

Figure 66: New antenna object creation

By default, the antenna created is a half-wavelength dipole. However, another antenna type can be selected from the large drop-down menu at the top. In this case, we will select an equiangular spiral antenna for the demonstration, like it can be seen in *Figure 67*.
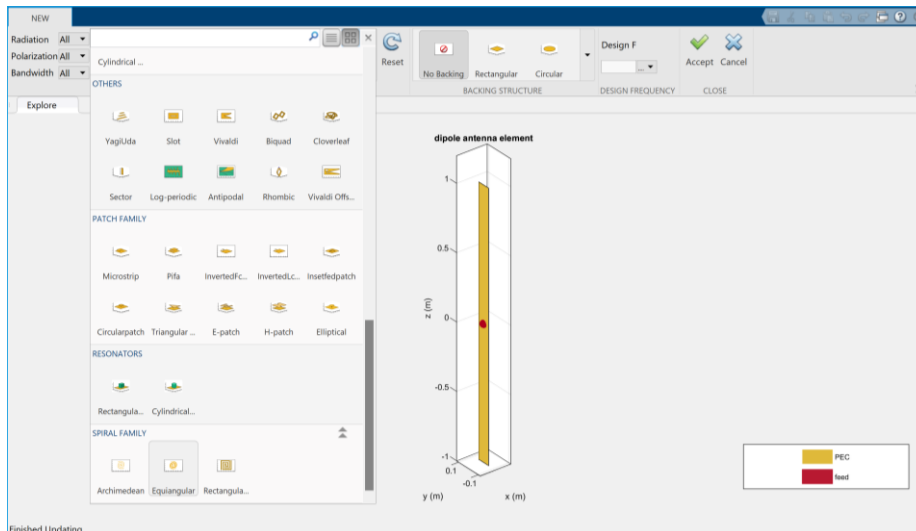
Figure 67: Antenna type selection

Once the antenna has been selected, the antenna representation will appear on the screen. The creation wizard also allows to adjust certain parameters, such as not considering the radiation in one direction or the creation of reflector elements. Once the parameters to simulate have been chosen, select the "Accept" button to continue.

By doing this, the selected antenna object itself is created. In the left panel, different parameters can be configured for the antenna. These parameters depend on the type of antenna selected, but usually include physical dimensions, tilt and orientation, the material from which the elements are made and the use of lumped loads. For the case of an equiangular spiral antenna, the parameters are as shown in *Figure 68*.
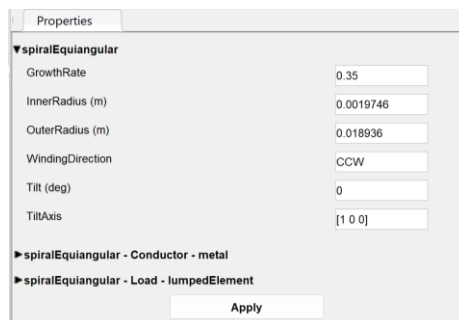

Figure 68: Antenna parameters editor

Once the parameters have been set, the element is created. The next step is to set both the frequency at which the simulations will be performed and the frequency range in which the simulations will be swept as a function of frequency. Once set, simulations can be obtained by simply selecting the corresponding buttons on the bar, as seen in *Figure 69*. The Optimize button is also available there, which is detailed below.
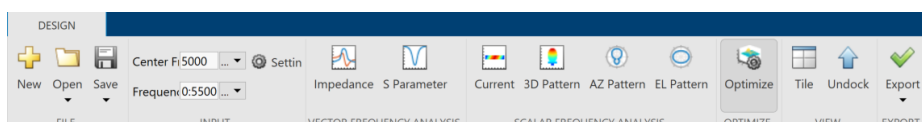

Figure 69: Generated antenna's options

49

Inside the Optimizer window, you will see different parameters to select. In the upper part of the window, the type of optimization to be performed can be selected: gain, F/B ratio, bandwidth, and physical dimensions of the antenna. It is also necessary to select the number of iterations to be performed and the optimization model, where it is recommended to leave the default one (SADEA). The left panel shows the same parameters that have been previously configured for the antenna. The physical parameters to be optimized must be selected, as well as the limits between which the model will iterate. For example, *Figure 70* sets the GrowthRate parameter as the only one to optimize. Once all the parameters have been configured, select the "Run" button to run the simulation.
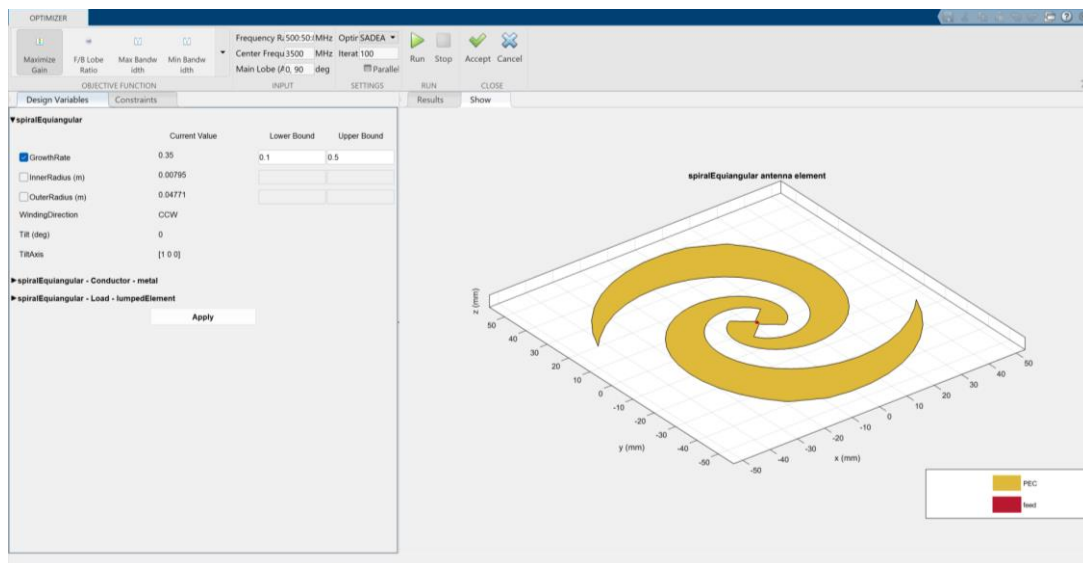

Figure 70: Antenna optimizer setup

First, the optimizer creates a model to follow, and then starts to iterate between the values set as limits (*Figure 71*). The simulation time will depend on factors such as the computational resources available to the user, the number of parameters to optimize and the number of iterations and model chosen for the optimization.
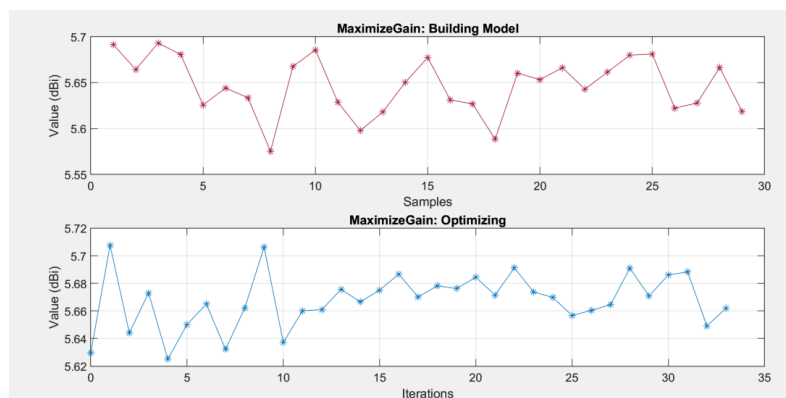

Figure 71: Graphical optimization status

Once the number of iterations reaches the number of iterations set at the beginning, the optimized parameters will appear below on the right. In this case, only the *GrowthRate* parameter of the equiangular spiral antenna has been optimized, obtaining a value of 0.14306, as seen in *Figure 72*.

50

Figure 72: Finished antenna optimization

Similarly, optimizations can be performed from code in the MATLAB terminal, without the need to run the Antenna Designer app. The code that performs the same optimization as the one performed by the graphical interface is as follows:

```
%Create an optimized antenna object
optAnt = optimize(spiralAnt, 3.5e9, 'maximizeGain', {'GrowthRate'}, {0.1;
0.5}, 'Iterations', 100)
```

The code requires an equiangular spiral antenna object, which is generated with the same code as in section 2.6. Once executed, a graph is displayed that allows knowing the status of the simulation (*Figure 73*). Once finished, the optimized parameter is saved in an antenna object of the same type as the one entered, called in this case arbitrarily *optAnt* (*Figure 74*), from which all the necessary simulations can be made following the code of section 2.6.
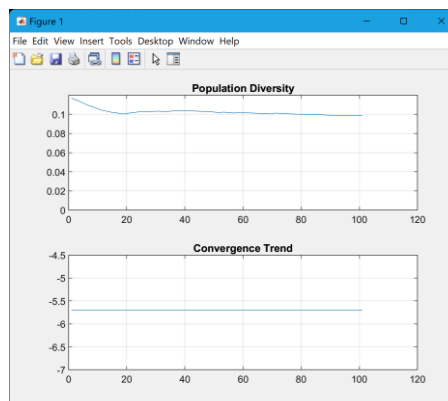
Figure 73: Command line optimization tool status

Figure 74: Optimized antenna object properties

6.2. Code to compare the growth rates of equiangular spiral antennas

```
%Create the antenna object with the first growth rate (N=0.5)
spiralAnt=spiralEquiangular;
spiralAnt.InnerRadius=0.00795;
spiralAnt.OuterRadius=0.04771;
spiralAnt.GrowthRate=0.57033475272;

%Store the azimuth-plane gain data
az11=patternAzimuth(spiralAnt,1.2E9);
```

51

```matlab
az12=patternAzimuth(spiralAnt,2.5E9);
az13=patternAzimuth(spiralAnt,2.5E9);
az14=patternAzimuth(spiralAnt,5.8E9);
az15=patternAzimuth(spiralAnt,8E9);

%Store the elevation-plane gain data
el11=patternElevation(spiralAnt,1.2E9);
el12=patternElevation(spiralAnt,2.5E9);
el13=patternElevation(spiralAnt,3.5E9);
el14=patternElevation(spiralAnt,5.8E9);
el15=patternElevation(spiralAnt,8E9);

%Store the S11 parameter, input impedance and axial ratio data
s1=sparameters(spiralAnt, 0.5E9:0.05E9:8E9);
z1=impedance(spiralAnt,0.5E9:0.05E9:8E9);
ar1=axialRatio(spiralAnt,0.5E9:0.05E9:8E9,0,90);

%Repeat the process for the second growth rate (N=1)
spiralAnt.GrowthRate=0.28516737636;

%Store the azimuth-plane gain data
az21=patternAzimuth(spiralAnt,1.2E9);
az22=patternAzimuth(spiralAnt,2.5E9);
az23=patternAzimuth(spiralAnt,2.5E9);
az24=patternAzimuth(spiralAnt,5.8E9);
az25=patternAzimuth(spiralAnt,8E9);

%Store the elevation-plane gain data
el21=patternElevation(spiralAnt,1.2E9);
el22=patternElevation(spiralAnt,2.5E9);
el23=patternElevation(spiralAnt,3.5E9);
el24=patternElevation(spiralAnt,5.8E9);
el25=patternElevation(spiralAnt,8E9);

%Store the S11 parameter, input impedance and axial ratio data
s2=sparameters(spiralAnt, 0.5E9:0.05E9:8E9);
z2=impedance(spiralAnt,0.5E9:0.05E9:8E9);
ar2=axialRatio(spiralAnt,0.5E9:0.05E9:8E9,0,90);

%Repeat the process for the third and final growth rate (N=2)
spiralAnt.GrowthRate=0.14258368818;

%Store the azimuth-plane gain data
az31=patternAzimuth(spiralAnt,1.2E9);
az32=patternAzimuth(spiralAnt,2.5E9);
az33=patternAzimuth(spiralAnt,2.5E9);
az34=patternAzimuth(spiralAnt,5.8E9);
az35=patternAzimuth(spiralAnt,8E9);

%Store the elevation-plane gain data
el31=patternElevation(spiralAnt,1.2E9);
el32=patternElevation(spiralAnt,2.5E9);
el33=patternElevation(spiralAnt,3.5E9);
el34=patternElevation(spiralAnt,5.8E9);
el35=patternElevation(spiralAnt,8E9);

%Store the S11 parameter, input impedance and axial ratio data
s3=sparameters(spiralAnt, 0.5E9:0.05E9:8E9);
z3=impedance(spiralAnt,0.5E9:0.05E9:8E9);
ar3=axialRatio(spiralAnt,0.5E9:0.05E9:8E9,0,90);

%Plot the azimuth plane polar pattern f=1.2GHz
p=polarpattern([az11 az21 az31],'Peaks',1,'TitleTop',"Azimuth plane Gain (dBi)
at 1.2GHz");
createLabels(p,'N≈%0.1f',[0.5 1 2]);
showPeaksTable(p, 1);
%f=2.5GHz
```

```matlab
p=polarpattern([az12 az22 az32],'Peaks',1,'TitleTop',"Azimuth plane Gain (dBi)
at 2.5GHz");
createLabels(p,'N≈%0.1f',[0.5 1 2]);
showPeaksTable(p, 1);
%f=3.5GHz
p=polarpattern([az13 az23 az33],'Peaks',1,'TitleTop',"Azimuth plane Gain (dBi)
at 3.5GHz");
createLabels(p,'N≈%0.1f',[0.5 1 2]);
showPeaksTable(p, 1);
f=5.8GHz
p=polarpattern([az14 az24 az34],'Peaks',1,'TitleTop',"Azimuth plane Gain (dBi)
at 5.8GHz");
createLabels(p,'N≈%0.1f',[0.5 1 2]);
showPeaksTable(p, 1);
f=8GHz
p=polarpattern([az15 az25 az35],'Peaks',1,'TitleTop',"Azimuth plane Gain (dBi)
at 8GHz");
createLabels(p,'N≈%0.1f',[0.5 1 2]);
showPeaksTable(p, 1);

%Plot the elevation plane polar pattern f=1.2GHz
p=polarpattern([el11 el21 el31],'Peaks',1,'TitleTop',"Elevation plane Gain
(dBi) at 1.2GHz");
createLabels(p,'N≈%0.1f',[0.5 1 2]);
showPeaksTable(p, 1);
%f=2.5GHz
p=polarpattern([el12 el22 el32],'Peaks',1,'TitleTop',"Elevation plane Gain
(dBi) at 2.5GHz");
createLabels(p,'N≈%0.1f',[0.5 1 2]);
showPeaksTable(p, 1);
%f=3.5GHz
p=polarpattern([el13 el23 el33],'Peaks',1,'TitleTop',"Elevation plane Gain
(dBi) at 3.5GHz");
createLabels(p,'N≈%0.1f',[0.5 1 2]);
showPeaksTable(p, 1);
%f=5.8GHz
p=polarpattern([el14 el24 el34],'Peaks',1,'TitleTop',"Elevation plane Gain
(dBi) at 5.8GHz");
createLabels(p,'N≈%0.1f',[0.5 1 2]);
showPeaksTable(p, 1);
%f=8GHz
p=polarpattern([el15 el25 el35],'Peaks',1,'TitleTop',"Elevation plane Gain
(dBi) at 8GHz");
createLabels(p,'N≈%0.1f',[0.5 1 2]);
showPeaksTable(p, 1);

%Plot the S11 parameters for the three growth rates
figure; hold on
rfplot(s1)
rfplot(s2)
rfplot(s3)
legend('N≈0.5','N≈1','N≈2');

%Plot the input resistances for the three growth rates
figure; hold on
plot(0.5E9:0.05E9:8E9,real(z1));
plot(0.5E9:0.05E9:8E9,real(z2));
plot(0.5E9:0.05E9:8E9,real(z3));
ylim([0 250]);
xlabel('Frequency (GHz)');
ylabel('Resistance (\Omega)');
legend('N≈0.5','N≈1','N≈2');
grid on;

%Plot the input reactances for the three growth rates
figure; hold on
plot(0.5E9:0.05E9:8E9,imag(z1));
plot(0.5E9:0.05E9:8E9,imag(z2));
```

```matlab
plot(0.5E9:0.05E9:8E9,imag(z3));
ylim([-100 100]);
xlabel('Frequency (GHz)');
ylabel('Reactance (\Omega)');
legend('N≈0.5','N≈1','N≈2');
grid on;

%Plot the axial ratios for the three growth rates
figure; hold on
plot(0.5E9:0.05E9:8E9,ar1);
plot(0.5E9:0.05E9:8E9,ar2);
plot(0.5E9:0.05E9:8E9,ar3);
ylim([0 10]);
xlabel('Frequency (GHz)');
ylabel('Axial ratio (dB)');
legend('N≈0.5','N≈1','N≈2');
grid on;
```

```matlab
plot(0.5E9:0.05E9:8E9,imag(z3));
ylim([-100 100]);
xlabel('Frequency (GHz)');
ylabel('Reactance (\Omega)');
```